August 2010, v. 38, no. 8

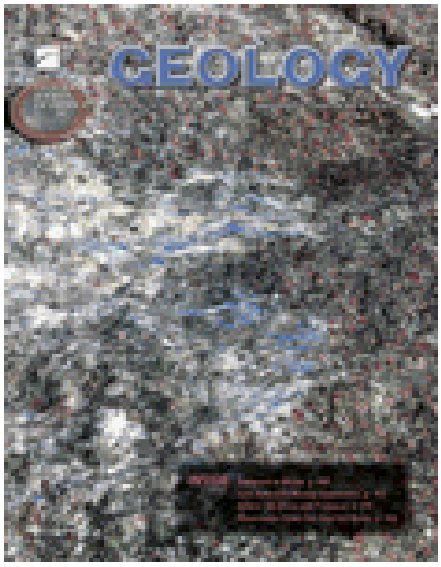

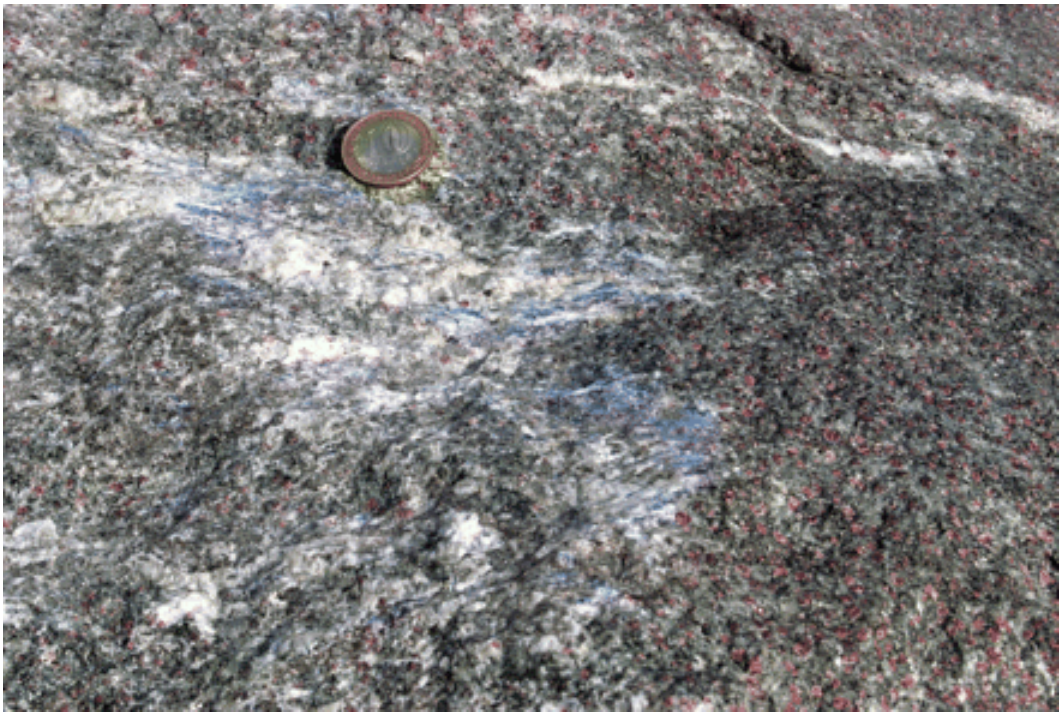

Cover image

Cover: Suprasubduction-type eclogite with crosscutting centimeter-scale veins and patches of garnet+kyanite+biotite plagiogranite, from the Mesoarchean Belomorian eclogite province of the Fennoscandian Shield (Chalma, Kola Peninsula, Russia). The Belomorian eclogite assemblage represents the oldest known example of high-pressure metamorphic rocks. See “Mesoarchean subduction processes: 2.87 Ga eclogites from the Kola Peninsula, Russia” by Mints et al., p. 739-742.

Photo by: Andrey A. Shchipansky

Cover design by: Heather L. Sutphin

Geology

Mesoarchean subduction processes: 2.87 Ga eclogites from the Kola Peninsula, Russia

M.V. Mints, E.A. Belousova, A.N. Konilov, L.M. Natapov, A.A. Shchipansky, W.L. Griffin, S.Y. O'Reilly, K.A. Dokukina and T.V. Kaulina

Geology 2010;38;739-742
doi: 10.1130/G31219.1

Notes

Mesoarchean subduction processes: 2.87 Ga eclogites from the Kola Peninsula, Russia

M.V. Mints[1], E.A. Belousova[2], A.N. Konilov[1], L.M. Natapov[2], A.A. Shchipansky[1], W.L. Griffin[2], S.Y. O'Reilly[2], K.A. Dokukina[1], and T.V. Kaulina[3]

[1]Geological Institute of Russian Academy of Sciences, Moscow 119017, Russia
[2]GEMOC ARC National Key Centre, Department of Earth and Planetary Sciences, Macquarie University, NSW 2109, Australia
[3]Geological Institute of the Kola Science Centre RAS, Apatity 184209, Russia

ABSTRACT

The nature of tectonic processes on the early Earth is still controversial. The scarcity of high-pressure metamorphic rocks such as eclogite (the high-pressure equivalent of basalt) in Archean cratons has been used to argue that plate tectonics did not operate until Earth had cooled to a critical point, perhaps around the 2.5 Ga Archean-Proterozoic transition. However, eclogites occur as meter- to kilometer-sized lenses enclosed in Archean gneisses of the Belomorian Province of the Fennoscandian shield. Geochemistry and internal features suggest that the protoliths of the eclogites were interlayered olivine gabbros, troctolites, and Fe-Ti oxide gabbros. Greenschist facies mineral parageneses are enclosed in prograde-zoned eclogite garnets, and peak metamorphic conditions define an apparent thermal gradient (12–15 °C/km), consistent with metamorphism in a warm Archean subduction zone. We show here that these eclogites represent the oldest known high-pressure metamorphic rocks. U-Pb dating and Hf isotope analyses of zircons from the eclogites and a crosscutting felsic vein define a minimum age of 2.87 Ga for the Uzkaya Salma eclogite; a 2.70 Ga age for the Shirokaya Salma eclogite is interpreted as the age of a granulite facies overprint. Thermal overprinting and growth of new zircon also occurred during the Svecofennian (1.9–1.8 Ga) orogeny. These new data imply that plate tectonic processes operated at least locally in late Mesoarchean time. The adakitic nature of the felsic vein suggests that partial melting of hydrated eclogites could produce Archean tonalite-trondhjemite-granodiorite–type magmas.

INTRODUCTION

The Archean continental crust is characterized by sodium-rich granitoids of the tonalite-trondhjemite-granodiorite (TTG) suite, and experimental studies suggest that these rocks were produced by partial melting of mafic protoliths containing residual amphibole and/or garnet (e.g., Wolf and Wyllie, 1994; Rapp and Watson, 1995). This melting could have occurred either in subduction environments (e.g., Martin, 1999; Moyen and Stevens, 2006) or at the base of thickened piles of mafic rocks similar to modern oceanic plateaus (e.g., Smithies et al., 2003). One of the major arguments against the Archean subduction model has been the apparent lack of Archean eclogites, which would represent the subducted, high-pressure equivalent of basaltic crust. This has led to speculation that plate tectonic processes (1) did not operate in the Archean, (2) operated differently (Davies, 1992), or that (3) high thermal gradients hindered eclogitization of mafic rocks (Bjørnerud and Austrheim, 2004).

Zircons from small eclogite bodies in a Neoarchean tectonic mélange near Gridino in Karelia (Russia; Fig. 1) were dated to 2721 ± 6 Ma (Volodichev et al., 2004). Many larger eclogite lenses have been recognized within gneisses in the Salma area, 210 km northwest of Gridino, along the southern margin of the Archean Kola continent within the tectonic province usually referred to as the Belomorian mobile belt (Konilov et al., 2004).

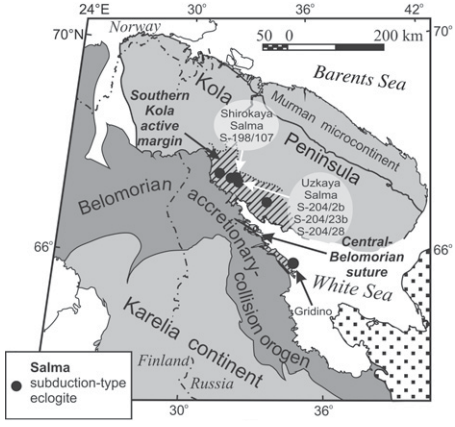

Figure 1. Schematic geological map of northwestern Fennoscandian shield, showing sample locations. (For detailed three-dimensional image of Belomorian belt, see Mints et al. [2009].)

GEOLOGICAL SETTING

The Belomorian tectonic province is a northwest-trending segment of the Archean nucleus of the Fennoscandian shield (Fig. 1; Fig. DR1 in the GSA Data Repository[1]). It was repeatedly affected by deformation and high- to moderate-pressure metamorphism in both Neoarchean and Paleoproterozoic time. The Keret' tectonic nappe that represents the southern margin of the Kola continent contains 2.89–2.70 Ga TTG gneisses and greenstones, and is separated from the Belomorian accretionary-collisional orogen by the Central Belomorian greenstone belt, a mafic-ultramafic sequence that is ca. 2.88–2.85 Ga or older (Bibikova et al., 1999).

The gneisses of the Keret' nappe enclose many small amphibolite bodies with or without garnet, previously interpreted as dismembered greenstones. Several of these bodies near the Salma Strait of Lake Imandra have been recognized as retrogressed eclogites (Konilov et al., 2004). They are lenses concordant with the TTG gneisses; their margins are retrograded to garnet-free amphibolites and they are cut by 1.9 Ga pegmatites. The Uzkaya Salma body is ~500 × 4000 m in outcrop, and the massive eclogite contains irregular layers and lenses of garnetite (Fig. DR2). Compositional and structural features of the eclogites suggest that the protoliths were intercalated Fe-Ti oxide gabbro and olivine gabbro with local troctolitic rocks, resembling the gabbroic suite from the modern oceanic crust of the Southwest Indian Ridge (Dick et al., 2000). The eclogites are cut by centimeter-scale veins and patches of garnet + kyanite + biotite plagiogranite. These may extend for several meters, have diffuse boundaries, and do not cross the eclogite-gneiss contact; at least some of them can be interpreted as partial melts of the eclogite, filling tension gashes. The Shirokaya Salma body is a pod of amphibolitized eclogite ~50 m across; the least retrograded rocks are massive eclogites.

SAMPLE DESCRIPTIONS

Detailed petrography and mineral chemistry will be presented elsewhere. The eclogites contain 3–5 mm almandine-pyrope garnets set in a matrix of vermicular clinopyroxene-plagioclase

[1]GSA Data Repository item 2010202, analytical methods, Figures DR1–DR3, and Tables DR1–DR4, is available online at www.geosociety.org/pubs/ft2010.htm, or on request from editing@geosociety.org or Documents Secretary, GSA, P.O. Box 9140, Boulder, CO 80301, USA.

symplectite; omphacite (up to Jd_{22} in Shirokaya Salma, Jd_{32} in Uzkaya Salma) is locally preserved (Fig. DR2). Quartz, rutile, and kyanite are minor phases. Secondary hornblende ± biotite are widespread. Some of the garnet porphyroblasts in the fine-grained clinopyroxene-plagioclase symplectite of the Uzkaya Salma eclogites grew in atoll fashion, and contain isolated inclusions of pumpellyite, actinolite, albite, titanite, hornblende, and zoisite, representing an armored pre-eclogite assemblage. Poikiloblastic garnets in eclogites show prograde zoning to more magnesian compositions, and 0.2 mm Fe-rich rims reflecting retrograde zoning. The Fe-Ti rocks are petrographically similar to the other eclogites, but contain more almandine-rich garnet and 5%–8% of ilmenite and magnetite. The garnetites contain minor rutile. The felsic vein consists of garnet, kyanite, and quartz, collar plagioclase ($An_{32–39}$) around kyanite, and minor biotite.

Typical rock compositions are given in Table DR1 (see the Data Repository). The eclogites cover a range of basaltic compositions; most have major and trace element compositions similar to typical normal mid-oceanic ridge basalt. The felsic veins are compositionally similar to the surrounding Archean TTG (Table DR1), and to the mean Phanerozoic adakite (i.e., SiO_2 > 56%, Al_2O_3 > 15%, MgO 2.4%–4.8%, Mg# 51–72; Smithies et al., 2003).

ZIRCON DATA

Zircons were separated from one sample of the Shirokaya Salma eclogite (S-198/107); the Uzkaya Salma outcrop is represented by one Fe-Ti eclogite (S-204–2B), one garnetite (S-204/23B), and a plagiogranite vein (S-204/28) in the eclogite. U-Pb ages (Fig. 2) were determined in situ by laser-ablation inductively coupled plasma–mass spectrometry (LA-ICP-MS) (Jackson et al., 2004), and Hf isotope compositions were analyzed in situ by LA-MC (multicollector)-ICP-MS (Griffin et al., 2000). Methods, results, and cathodoluminescence (CL) images of zircons are given in Tables DR2 and DR3 and Figure DR3.

Zircons from the Fe-Ti eclogite are irregular to subhedral, and contain abundant black inclusions. They are cracked and featureless in CL images, and appear to be partially metamict. They are similar to zircon grains precipitated from trapped intercumulus liquid in Fe-Ti gabbro dikes from the Lanzo lherzolitic massif, northern Italy (Kaczmarek et al., 2008). The U-Pb analyses of 13 grains show two concordant grains at 2820 Ma and one at 1913 Ma; the remaining grains give $^{207}Pb/^{206}Pb$ ages between these two intercepts. All of these grains have similar Hf-isotope compositions (Fig. 3); those of the oldest grains are closer to the depleted mantle evolution line, and we infer that an original population with ages of ca. 2820 Ma or older was partially reset during the Svecofennian orogeny (1.8–1.9 Ga).

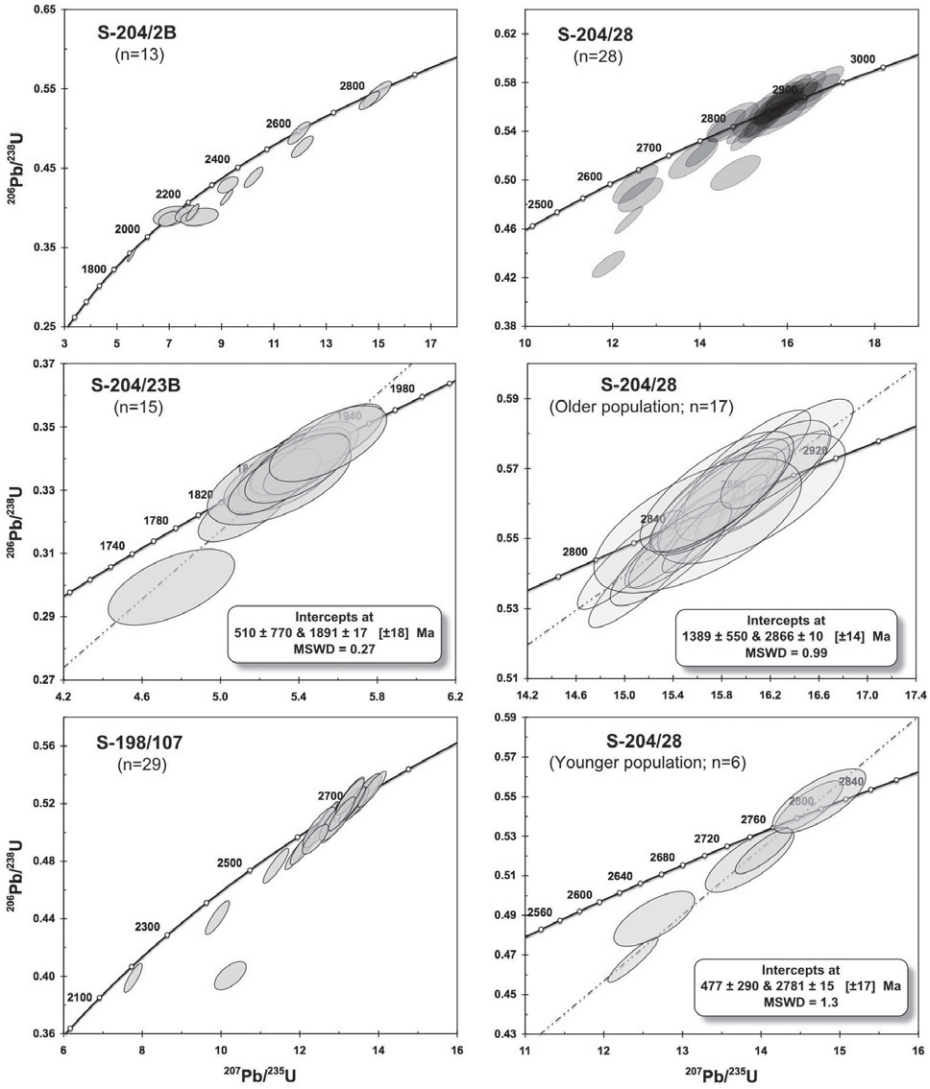

Figure 2. Concordia diagrams for analyzed samples. MSWD—mean square of weighted deviates.

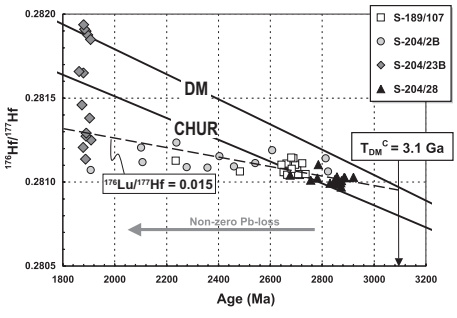

Figure 3. Plot of U/Pb age vs. $^{176}Hf/^{177}Hf$ shows relatively narrow horizontal band of points that suggests resetting of U-Pb system, where zircons with younger U-Pb ages clearly have been affected by non-zero Pb loss (ca. 1.9 Ga). T_{DM}^{C}—crustal modal age.

Zircons from the garnetite are irregular to tabular, and 50 × 100 µm. Many have inclusion-filled cores similar to the zircons of the Fe-Ti eclogite, surrounded by broad structureless cracked rims. The U-Pb analyses show a single population of concordant to near-concordant grains with a concordia age of 1891 ± 17 Ma (mean square of weighted deviates, MSWD = 0.27; Fig. 2) and an error-weighted mean $^{207}Pb/^{206}Pb$ age of 1887 ± 18 Ma (MSWD = 0.14). Unlike the other samples, this population shows a large range in εHf, from −14 to +14. The lowest values are similar to those of the eclogite and the plagiogranite vein; the highest are well above the depleted mantle evolution line.

Ovoid zircons from the Shirokaya Salma eclogite show core-rim zoning, but core-rim analyses of three grains showed no age difference. Of 26 grains, 18 are concordant and yield an error-weighted mean $^{207}Pb/^{206}Pb$ age of 2703 ± 9 Ma (MSWD = 0.53). Their Hf-isotope compositions are similar to those of the Uzkaya Salma Fe-Ti eclogite (εHf = 1–4). Several discordant grains have identical Hf isotope

compositions, suggesting Pb loss during a Proterozoic metamorphic event.

Zircons from the Uzkaya Salma plagiogranite (S-204/28) are subhedral 50 × 100 µm grains with clear core-rim structures in CL images; the cores display fine oscillatory zoning, typical of magmatic zircons, while the 10–20 µm rims are featureless, cracked, and apparently metamict. The 28 U-Pb analyses of 26 grains define two distinct age populations. The older population has an upper intercept of 2866 ± 10 Ma (MSWD = 0.99; Fig. 2). The younger population (6 grains) is more discordant, and gives an upper-intercept age of 2781 ± 15 Ma (MSWD = 1.3). The εHf of the older population is +3 to +4, indicating a juvenile origin; the younger population has similar Hf isotope compositions, suggesting that their ages reflect resetting (nonzero Pb loss) of the older zircons, perhaps ca. 2.78 Ga (Fig. 3).

DISCUSSION AND CONCLUSIONS

The felsic veins in the Uzkaya Salma eclogite crosscut the internal layering of the eclogite and constrain the eclogite metamorphism to ca. 2.87 Ga or older; this is the oldest eclogite yet reported. The juvenile Hf isotope composition of these zircons is consistent with an origin by partial melting of a protolith recently derived from the depleted mantle (maximum model age, assuming an average crustal Lu/Hf, is ca. 3.1 Ga; Fig. 3).

The poor quality of the zircon grains in the Uzkaya Salma Fe-Ti eclogites hinders precise dating. However, the oldest ages (2.82 ± 0.04 Ga) are within error of the age of the crosscutting felsic veins. Sensitive high-resolution ion microprobe analyses of zircons from the same sample yield an upper intercept of 2885 ± 45 Ma and one concordant grain gives an age of 2891 ± 50 Ma (Kaulina et al., 2007; Table DR2B). These zircons of probable magmatic origin were affected by a later metamorphic event, which may be recorded by the 1891 ± 17 Ma metamorphic zircons of the garnetites. Their large range of εHf suggests that the zircons in the garnetite were generated by the local breakdown of older Zr-bearing minerals with a range of Lu/Hf, like zircons from garnetite xenoliths in basalts of the Four Corners area of the United States (Smith and Griffin, 2005). The age of the garnetite zircons corresponds to the Svecofennian orogeny, when imbricate thrusting brought deep-seated rocks of the Belomorian belt to shallower levels (Bibikova et al., 2004).

Zircons from the Shirokaya Salma eclogite appear to be 150–170 m.y. younger than the zircons from Uzkaya Salma, and close in age to the morphologically similar zircons of the eclogites at Gridino (Volodichev et al., 2004), 210 km to the southeast (Fig. 1). Our petrological study of the eclogites shows that the retrograde portion of the pressure-temperature-time (*P-T-t*) path crossed through the granulite facies *P-T* space, producing clinopyroxene-orthopyroxene mineral assemblages (Fig. 4). The morphology and geochemical features of the 2.7 Ga zircons suggest that this age reflects metamorphic growth of new zircon crystals during the retrograde granulite facies metamorphism.

The low-grade mineral assemblage preserved in the cores of garnets in the Uzkaya Salma eclogite indicates pre-eclogite *P-T* conditions of 340–380 °C at 0.6–0.9 GPa (Konilov, 2008). Coexisting garnet and omphacite give peak metamorphic conditions of ~700 °C at 1.3 (Shirokaya Salma) to ≥1.4 GPa (Uzkaya Salma). The pressure estimates are minimum values; garnet-kyanite-plagioclase barometry and the presence of rutile in the plagiogranites suggest *P* >1.5 GPa (Xiong et al., 2005). Analyses of garnet rims and the clinopyroxene-plagioclase-quartz coronas suggest conditions of 700–750 °C and 0.8–1.3 GPa during the retrograde stage (Fig. 4; Fig. DR2; Table DR4). This may reflect rapid uplift of the subducted material during extension ca. 2.7 Ga, but it may also reflect the later Svecofennian metamorphism. The clockwise *P-T* path is similar to those recorded by many eclogites from Phanerozoic subduction settings (e.g., Page et al., 2003). The peak metamorphic conditions suggest a geothermal gradient of 12–15 °C/km; this is somewhat higher than those predicted for the upper surfaces of modern subducting slabs (Peacock et al., 2002), and may reflect warmer conditions in the Archean mantle. Brown (2006, 2009) argued that the first appearance of this eclogite–high-*P* granulite–type of metamorphism reflects the initiation of subduction, in an early style of plate tectonics that became global in late Neoarchean time and dominated until the Neoproterozoic, when modern-style plate tectonics characterized by ultrahigh-*P* metamorphism began (Stern, 2005). The Belomorian eclogites described here provide evidence that the transition to a recognizable plate tectonic regime began, at least locally, as early as 2.8–2.9 Ga. This also supports the inference (Moyen et al., 2006) of Mesoarchean subduction, based on studies in the Barberton granitoid-greenstone terrane.

The Uzkaya Salma plagiogranites are compositionally similar to the adjacent TTG gneisses (Table DR1); both are broadly similar to modern adakites, and to experimental melts produced from hydrated eclogite at *P* ≥1.5 GPa (Prouteau et al., 1999). Such melts could be generated by partial melting of an eclogite at the peak metamorphic temperature (~700 °C) only if water was present (Prouteau et al., 1999), implying subduction of water into the upper mantle, probably within the ultramafic part of the slab (Scambelluri and Philippot, 2001). The example of the Uzkaya Salma eclogite suggests that TTG-type melts could have been generated in subduction-zone settings in late Mesoarchean time.

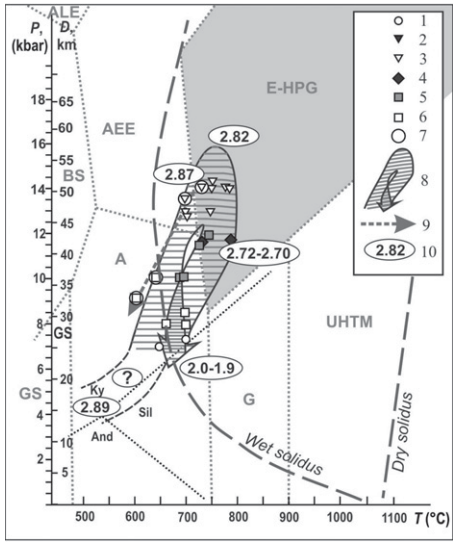

Figure 4. Inferred pressure-temperature-time (*P-T-t*) path for metamorphic evolution of Salma eclogite. D—depth. Metamorphic facies (after Brown, 2009): BS—blueschist, AEE—amphibole-epidote eclogite, ALE—amphibole-lawsonite eclogite, GS—greenschist, A—amphibolite, G—granulite facies, E-HPG—medium-*T* eclogite–high-*P* granulite metamorphism, UHTM—ultrahigh-*T* metamorphic part of granulite facies. Data in Table DR4 (see footnote 1) are basis for *P-T-t* path and metamorphic stages: 1—prograde; 2, 3—eclogite, 4—retrograde granulite; 5, 6—retrograde amphibolite; 7 (in circles)—plagiogranites. *P-T-t* trajectories: 8—eclogite, 9—plagiogranite. Points for *P-T* equilibriums based on independent *P* and *T* estimates are marked by closed symbols; points based on single estimate of one parameter and suggested value for second parameter are marked by open symbols; 10—age of main metamorphic events (in Ga).

ACKNOWLEDGMENTS

We are grateful to Norman Pearson for his constant assistance with the analytical work, and for direction of the laboratory. Analytical data were obtained at GEMOC (Geochemical Evolution and Metallogeny of Continents) using instrumentation funded by Australian Research Council Linkage Infrastructure, Equipment and Facilities (ARC LIEF), and Department of Education Science and Training (DEST) Systemic Infrastructure Grants, and Macquarie University. This is contribution 652 from the GEMOC ARC National Key Centre (www.es.mq.edu.au/GEMOC/). We are grateful to the Russian Foundation for Basic Research, projects 06-05-65237, 07-05-00292, 07-05-00759, 08-05-00350, 09-05-01006, and also to the Russian Science Support Foundation for financial support of the field, geochemical, and petrological studies. This work contributes to Program 6 of the Earth Sciences Department of the Russian Academy of Sciences.

REFERENCES CITED

Bibikova, E.V., Slabunov, A.I., Bogdanova, S.V., Skiöld, T., Stepanov, V.S., and Borisova, E.Y., 1999, Early magmatism of the Belomorian

mobile belt: Lateral zoning and isotope age: Petrology, v. 7, no. 2, p. 115–140.
Bibikova, E.V., Bogdanova, S.V., Glebovitsky, V.A., Claesson, S., and Skiöld, T., 2004, Evolution stages of the Belomorian mobile belt from U-Pb zircon geochronology (NORDSIM ion microprobe): Petrology, v. 12, no. 3, p. 195–210.
Bjørnerud, M.G., and Austrheim, H., 2004, Inhibited eclogite formation: The key to the rapid growth of strong and buoyant Archean continental crust: Geology, v. 32, p. 765–768, doi: 10.1130/G20590.1.
Brown, M., 2006, Duality of thermal regimes is the distinctive characteristic of plate tectonics since the Neoarchean: Geology, v. 34, p. 961–964, doi: 10.1130/G22853A.1.
Brown, M., 2009, Metamorphic patterns in orogenic systems and the geological record, *in* Cawood, P.A., and. Kröner, A., eds., Earth accretionary systems in space and time: Geological Society of London Special Publication 318, p. 37–74.
Davies, G.F., 1992, On the emergence of plate tectonics: Geology, v. 20, p. 963–966, doi: 10.1130/0091-7613(1992)020<0963:OTEOPT>2.3.CO;2.
Dick, H.J.B., and 27 others, 2000, A long in situ section of the lower ocean crust: Results of ODP Leg 176 drilling at the Southwest Indian Ridge: Earth and Planetary Science Letters, v. 179, p. 31–51, doi: 10.1016/S0012-821X(00)00102-3.
Griffin, W.L., Pearson, N.J., Belousova, E., Jackson, S.E., O'Reilly, S.Y., van Achterberg, E., and Shee, S.R., 2000, The Hf isotope composition of cratonic mantle: LAM-MC-ICPMS analysis of zircon megacrysts in kimberlites: Geochimica et Cosmochimica Acta, v. 64, p. 133–147, doi: 10.1016/S0016-7037(99)00343-9.
Jackson, S.E., Pearson, N.J., Griffin, W.L., and Belousova, E.A., 2004, The application of laser ablation-inductively coupled plasma-mass spectrometry to in-situ U-Pb zircon geochronology: Chemical Geology, v. 211, p. 47–69, doi: 10.1016/j.chemgeo.2004.06.017.
Kaczmarek, M.-A., Müntener, O., and Rubatto, D., 2008, Trace element chemistry and U-Pb dating of zircons from oceanic gabbros and their relationship with whole rock composition (Lanzo, Italian Alps): Contributions to Mineralogy and Petrology, v. 155, p. 295–312, doi: 10.1007/s00410-007-0243-3.
Kaulina, T.V., Apanasevich, E.A., Savchenko, E.E., Sergeev, S.A., Presnyakov, S.V., Shchipansky, A.A., and Yapaskurt, V.O., 2007, Archean eclogites of the Belomorian belt: Results of U-Pb and Sm-Nd dating of garnets and U-Th-Pb (SHRIMP) dating of zircons, *in* Voitekhovsky, Yu.L., ed., Geology and mineralogy of the Kola region: Proceedings of the Science meeting: Apatity, Russia, K & M, p. 229–232 (in Russian).
Konilov, A., 2008, Prograde history of the Archean Salma eclogites and piclogites (Belomorian eclogite province) [abs.], *in* MPN-02 Metamorphism and metamorphic processes: Oslo, Norway, 33rd International Geological Congress 2008 (CD-ROM).
Konilov, A.N., Shchipansky, A.A., Mints, M.V., and Volodichev, O.I., 2004, Petrology of eclogites of the Belomorian Province: Florence, Italy, 32nd International Geological Congress 2004, Abstracts, Part 1, p. 108.
Martin, H., 1999, Adakitic magmas: Modern analogues of Archaean granitoids: Lithos, v. 46, p. 411–429, doi: 10.1016/S0024-4937(98)00076-0.
Mints, M., Suleimanov, A., Zamozhniaya, N., and Stupak, V., 2009, A three-dimensional model of the early Precambrian crust under the southeastern Fennoscandian Shield: Karelia craton and Belomorian tectonic province: Tectonophysics, v. 472, p. 323–339, doi: 10.1016/j.tecto.2008.12008.
Moyen, J.-F., and Stevens, G., 2006, Experimental constraints on TTG petrogenesis: Implications for Archean geodynamics, *in* Benn, K., et al., eds., Archean geodynamics and environments: American Geophysical Union Geophysical Monograph 164, p. 149–175.
Moyen, J.-F., Stevens, G., and Kisters, A., 2006, Record of mid-Archaean subduction from metamorphism in the Barberton terrain, South Africa: Nature, v. 442, p. 559–562, doi: 10.1038/nature04972.
Page, F.Z., Essene, E.J., and Mukasa, S.B., 2003, Prograde and retrograde history of eclogites from the Eastern Blue Ridge, North Carolina, USA: Journal of Metamorphic Geology, v. 21, p. 685–698, doi: 10.1046/j.1525-1314.2003.00479.x.
Peacock, S.M., Wang, W., and McMahon, A.M., 2002, Thermal structure and metamorphism of subducting oceanic crust: Insight into Cascadia intraslab earthquakes, *in* Kirby, S., et al., eds., The Cascadia subduction zone and related subduction systems: U.S. Geological Survey Open-File Report 02-328, p. 123–126.
Prouteau, G., Scaillet, B., Pichavant, M., and Maury, R.C., 1999, Fluid-present melting of oceanic crust in subduction zones: Geology, v. 27, p. 1111–1114, doi: 10.1130/0091-7613(1999)027<1111:FPMOOC>2.3.CO;2.
Rapp, R.P., and Watson, E.B., 1995, Dehydration melting of metabasalt at 8–32 kbar: Implications for continental growth and crust-mantle recycling: Journal of Petrology, v. 36, p. 891–931, doi: 10.1093/petrology/36.4.891.
Scambelluri, M., and Philippot, P., 2001, Deep fluids in subduction zones: Lithos, v. 55, p. 213–227, doi: 10.1016/S0012-821X(97)00043-5.
Smith, D., and Griffin, W.L., 2005, Garnetite xenolith and mantle-water interactions below the Colorado Plateau, southwestern US: Journal of Petrology, v. 46, p. 901–1924, doi: 10.1093/petrology/egi042.
Smithies, R.H., Champion, D.C., and Cassidy, K.F., 2003, Formation of Earth's early Archean continental crust: Precambrian Research, v. 127, p. 89–101, doi: 10.1016/S0301-9268(03)00182-7.
Stern, R.J., 2005, Evidence from ophiolites, blueschists and ultrahigh-pressure metamorphic terranes that the modern episode of subduction tectonics began in Neoproterozoic time: Geology, v. 33, p. 557–560, doi: 10.1130/G21365.1.
Volodichev, O.I., Slabunov, A.I., Bibikova, E.V., Konilov, A.N., and Kuzenko, T.I., 2004, Archean eclogites in the Belomorian mobile belt, Baltic Shield: Petrology, v. 12, p. 540–560.
Wolf, M.B., and Wyllie, P.J., 1994, Dehydration melting of amphibolite at 10 kbar: The effects of temperature and time: Contributions to Mineralogy and Petrology, v. 115, p. 369–383, doi: 10.1007/BF00320972.
Xiong, X.L., Adam, J., and Green, T.H., 2005, Rutile stability and rutile/melt partitioning during partial melting of hydrous basalt: Implication for TTG genesis: Chemical Geology, v. 218, p. 339–359, doi: 10.1016/j.chemgeo.2005.01.014.

Manuscript received 2 November 2009
Revised manuscript received 17 March 2010
Manuscript accepted 20 March 2010

Printed in USA

ANALYTICAL METHODS

U-Pb dating

Samples and standards were acid-washed before being analysed to remove possible surface Pb contamination. The grains were analysed using a commercial LUV213 laser ablation system (λ = 213nm) (New Wave/Merchantek), attached to a Hewlett Packard 4500s ICPMS (Jackson et al., 2004). All ablations were carried out in He. Ablation pits were about 50 μm in diameter. The time-resolved signals were processed using the GLITTER interactive software to select the portions of the grains that had suffered least lead loss, or gain of common Pb, and were thus closest to being concordant. U-Pb isotopic data results are given in Table 2.

The standard used in this work is the GEMOC-GJ-1 gem zircon (Elhlou et al., 2006), with a TIMS age of 608.5 Ma. This standard is run 2-4 times before and after each ten unknowns. Cross-analysis of other international standards also gives good results. Two analyses of Mud Tank zircon (734±32 Ma; Black and Gulson, 1978) and two of zircon 91500 (1064 Ma; Wiedenbeck et al., 1995) were run during this work, and their mean values are within 1 s.d. of the recommended values.

U-Pb data for some well-characterised zircons

Zircon	TIMS 207/206	206/238	207/235	207/206
91500	**1065.4**	Wiedenbeck, et al. (1995; n=11)		
This study n=9		1067±3	1065±4	**1061±8**
Long-term work* n=83		1061±36	1063±29	**1068±26**
Mud Tank	**734±32**	Black & Gulson (1978; n=5)		
This study n=9		**726±5**	729±7	737±16
Long-term work* n=73		**733±14**	735±8	739±12

* Jackson et al., 2004

Hf-isotope analyses

Hf isotope analyses were carried out *in situ* with a UP 213 laser-ablation microprobe, attached to a Nu Plasma multi-collector ICPMS at GEMOC, Macquarie University. Most analyses were carried out with a beam diameter of ca 50 μm, a 4 Hz repetition rate, and energies of 0.1 mJ/pulse and 0.6 J/cm^2. Typical ablation times were 80-120 s, resulting in pits 40-60 μm deep. The methodology and analyses of standard solutions and standard zircons are described by Griffin *et al.* (2000).

The measured $^{176}Lu/^{177}Hf$ ratios are used to calculate initial $^{176}Hf/^{177}Hf$ ratios. The typical 2SE uncertainty on a single analysis of $^{176}Lu/^{177}Hf$ is ±1-2%, reflecting both analytical uncertainties and the spatial variation of Lu/Hf across many zircons; at the Lu/Hf ratios considered here, this contributes an uncertainty of <0.1 ε_{Hf} unit. For the calculation of ε_{Hf} values, we have adopted the chondritic values of Blichert-Toft et al.

(1997). To calculate model ages (T_{DM}) based on a depleted-mantle source, we have adopted a model with $^{176}Hf/^{177}Hf)_i = 0.279718$ and $^{176}Lu/^{177}Hf = 0.0384$; this produces a value of $^{176}Hf/^{177}Hf$ (0.28325) similar to that of average MORB over 4.56 Ga. There are currently several values of the decay constant for ^{176}Lu: 1.93 x 10-11yr^{-1} proposed by Blichert-Toft et al.,1997; 1.865 x 10-11yr^{-1} by Scherer et al., 2001; and 1.983 x 10-11yr^{-1} by Bizzarro et al., 2003; calculations using these are provided in Table 3. Values used in Figure 4 have been calculated using the decay constant proposed by Scherer *et al*. (2001).

T_{DM} ages, which are calculated using the measured $^{176}Lu/^{177}Hf$ of the zircon, can only give a minimum age for the source material of the magma from which the zircon crystallised. Therefore we also have calculated, for each zircon, a "crustal" model age (T_{DM}^{C}; Table 3) which assumes that its parental magma was produced from an average continental crust ($^{176}Lu/^{177}Hf = 0.015$) that originally was derived from the depleted mantle.

References

Bizzaro,M., Baker, J.A., Haack, H., Ulfbeck, D. & Rosing, M. Early History of Earth 's crust-mantle system inferred from hafnium isotope in chondritis. Nature 421, 931-933 (2003).

Black L.P. & Gulson, B.L. The age of Mud Tank carbonatite, Strangways Range, North Territory. BMR Journal of Australian Geol. and Gephys. 3, 227-232 (1978).

Blichert-Toft, J., Chauvel, CC. & Albaréde, F. The Lu-Hf geochemistry of hondritesand the evolution of the mantle-cust system. Earth and Planet. Sci, Letters, 148, 243-258. Erratum. Eart and Planet. Sci. Letters 154, 349 (1997).

Elhlou, S., Belousova, E.A., Griffin, W. L., Pearson, N. J. & O'Reilly, S.Y. Trace element and isotopic composition of GJ red zircon standard by Laser Ablation. Conference Abstract. Geochim. Cosmochim. Acta 70 (18), p. A158 (2006).

Griffin, W.L. et al. The Hf isotope composition of cratonic mantle: LAM-MC-ICPMS analysis of zircon megacrysts in kimberlite. Geochim. Cosmochim. Acta 64, 133-147 (2000).

Jackson, S. E., Pearson, N.J., Griffin, W.L. & Belousova, E.A. The application of laser ablation microprobe-inductively coupled plasma-mass spectrometry (LAM-ICP-MS) to in situ U-Pb zircon geochronology. Chem. Geol. 211, 47-69 (2004).

Scherer, E., Münker, C. & Mezger, K.,. Calibration of the lutetium-hafnium clock. Science 293, 683-687 (2001).

Wiedenbeck, M. et al. The natural zircon standarts for U-Th-Pb, Lu-Hf, trace-element and REE analyses. Geostands Newsletter 19, 1-23 (1995).

Table DR1. Major and trace element composition of the studied rock types

Type of rock	**eclogite/ ShS**	**Fe-Ti eclogite/UzS**	**garnetite/ UzS**	**plagiogranite/ UzS**	**TTG gneiss/ UzS**	**TTG gneiss/ ShS**
Sample N	S-198/107	S-204/2b	S-204/23b	S-204/28	SB-810	KV-05/6
Age (Ga)	2.7	2.82	1.89	2.86	2.74*	2.96*
Major elements (wt%)						
SiO_2	49.98	45.62	43.8	68.34	68.5	63.6
TiO_2	0.76	2.22	1.34	0.49	0.41	0.63
Al_2O_3	15.06	13.92	17.4	15.19	15.8	15.9
Fe_2O_3	12.24	20.81	19.9	4.29	3.34	5.23
MnO	0.19	0.24	0.26	0.05	0.05	0.09
MgO	8.54	5.45	6.14	1.84	1.32	2.61
CaO	10.92	9.93	10.1	4.77	3.55	4.97
Na_2O	1.88	1.86	1.15	2.93	4.7	4.11
K_2O	0.31	0.03	0.07	0.06	1.76	2.17
P_2O_5	0.07	0.05	<0.05	0.11	0.11	0.18
LOI	0.13	0.22	<1	0.52	0.28	0.35
Sum	**100.08**	**100.00**	**100.00**	**100.15**	**99.82**	**99.84**
Mg#	0.63	0.38	0.2	0.5	0.48	0.53
Trace elements (ppm)						
Sc	49	44	59.1	7	-	-
V	216	1170	512	54	38	46
Cr	478	6.5	24.2	37	8	12
Co	47.3	84	-	20	9	8.5
Ni	-	26	42.2	35	-	-
Rb	3.53	0.74	2.86	40	70	71
Sr	50.6	41	34.5	404	434	309
Y	16.6	28.9	25.9	8.9	6.87	7.4
Zr	43.4	77.1	39.5	227	146	147
Nb	2.46	3.75	1.84	6.72	6.1	5.71
Ba	25.7	5	22.5	536	627	529
La	1.41	0.76	0.31	25.4	30.8	22.2
Ce	4.49	2.31	0.35	50.5	57.6	43.2
Pr	0.71	0.44	0.08	5.54	6.46	4.53
Nd	3.84	3.22	0.52	20.2	21.5	15.9
Sm	1.34	2.16	0.7	3.6	3.18	2.81
Eu	0.44	1.04	0.49	1.29	0.85	0.75
Gd	1.63	3.29	2.41	3.34	2.54	2.55
Tb	0.36	0.76	0.66	0.45	0.34	0.34
Dy	2.64	4.95	4.23	2.04	1.5	1.67
Ho	0.63	1.07	0.91	0.34	0.27	0.29
Er	1.86	3.22	2.55	0.71	0.61	0.73
Tm	0.25	0.44	0.36	0.12	0.09	0.1
Yb	1.77	2.93	2.59	0.7	0.56	0.61
Lu	0.24	0.46	0.39	0.11	0.07	0.09
Hf	1.23	2.1	1.27	5.1	3.84	3.69
Ta	0.14	0.23	0.1	0.51	0.26	0.28
Th	0.08	0.13	<0.1	4.13	3.82	3.14
U	0.04	0.07	<0.1	1.14	0.29	0.28

* unpublished data of M. Mints et al., SHRIMP-II

Mg# = $Mg/(Mg+Fe^{2+})$

Table DR2A. Zircon LAM-ICPMS U-Pb isotopic data

Analysis #	$^{207}Pb/^{206}Pb$	± 1 σ	$^{207}Pb/^{235}U$	± 1 σ	$^{206}Pb/^{238}U$	± 1 σ	$^{208}Pb/^{232}Th$	± 1 σ	$^{207}Pb/^{206}Pb$ age	± 1 σ	$^{207}Pb/^{235}U$ age	± 1 σ	$^{206}Pb/^{238}U$ age	± 1 σ	$^{208}Pb/^{232}Th$ age	± 1 σ	Th(ppm)	U(ppm)
Sample: S198/107																		
S198/107-01	0.1810	0.0020	12.72	0.12	0.5098	0.0042	0.1432	0.0025	2662	18	2659	9	2656	18	2704	44	110	828
S198/107-02	0.1854	0.0021	13.23	0.13	0.5178	0.0047	0.1405	0.0028	2702	19	2697	9	2690	20	2658	49	53	353
S198/107-03	0.1869	0.0021	13.50	0.13	0.5242	0.0047	0.1437	0.0027	2715	19	2715	9	2717	20	2714	47	68	362
S198/107-05	0.1807	0.0021	12.69	0.14	0.5093	0.0049	0.1468	0.0032	2659	20	2657	10	2654	21	2769	57	76	617
S198/107-06	0.1849	0.0020	13.24	0.12	0.5194	0.0045	0.1457	0.0023	2697	18	2697	9	2696	19	2750	40	57	417
S198/107-07	0.1855	0.0020	13.35	0.13	0.5220	0.0046	0.1448	0.0023	2703	18	2705	9	2708	20	2733	41	75	513
S198/107-09	0.1876	0.0024	13.57	0.18	0.5247	0.0057	0.1424	0.0039	2721	22	2720	12	2719	24	2691	69	47	146
S198/107-10	0.1878	0.0023	13.72	0.15	0.5298	0.0046	0.1475	0.0037	2723	21	2730	10	2740	19	2781	64	28	67
S198/107-11	0.1868	0.0023	13.39	0.15	0.5197	0.0049	0.1472	0.0036	2714	21	2707	11	2698	21	2776	63	55	377
S198/107-14Core	0.1856	0.0022	13.31	0.14	0.5202	0.0048	0.1461	0.0034	2704	20	2702	10	2700	20	2756	60	183	814
S198/107-14Rim	0.1846	0.0035	10.23	0.16	0.4020	0.0040	0.1105	0.0012	2695	32	2456	15	2178	18	2118	22	26	193
S198/107-15Core	0.1801	0.0019	12.68	0.12	0.5105	0.0046	0.1439	0.0022	2654	18	2656	9	2659	20	2717	38	84	534
S198/107-15Rim	0.1781	0.0026	11.95	0.13	0.4865	0.0048	0.1342	0.0014	2635	25	2600	10	2556	21	2545	25	120	665
S198/107-16	0.1848	0.0021	12.86	0.13	0.5049	0.0047	0.1363	0.0026	2696	19	2670	10	2635	20	2583	47	201	911
S198/107-17	0.1730	0.0020	11.39	0.13	0.4775	0.0049	0.1342	0.0029	2587	20	2556	11	2516	22	2546	52	93	731
S198/107-18	0.1789	0.0022	12.10	0.14	0.4906	0.0051	0.1396	0.0032	2643	21	2612	11	2573	22	2641	56	39	103
S198/107-19	0.1864	0.0021	13.36	0.13	0.5199	0.0045	0.1421	0.0028	2710	19	2705	9	2699	19	2686	50	56	376
S198/107-20	0.1893	0.0022	13.84	0.15	0.5302	0.0050	0.1433	0.0029	2736	19	2739	10	2742	21	2707	51	76	431
S198/107-21	0.1847	0.0021	13.21	0.13	0.5188	0.0046	0.1432	0.0027	2696	19	2695	9	2694	20	2705	48	116	730
S198/107-22	0.1840	0.0021	13.19	0.12	0.5200	0.0044	0.1415	0.0026	2689	19	2694	9	2699	19	2674	47	119	456
S198/107-23	0.1626	0.0021	9.90	0.12	0.4418	0.0047	0.1256	0.0030	2483	22	2426	12	2359	21	2392	53	59	101
S198/107-24	0.1798	0.0024	12.49	0.17	0.5040	0.0057	0.1324	0.0038	2651	22	2642	13	2631	24	2513	68	90	495
S198/107-25Core	0.1831	0.0021	13.27	0.15	0.5258	0.0053	0.1387	0.0029	2681	20	2699	11	2724	22	2626	52	82	247
S198/107-25Rim	0.1843	0.0025	12.92	0.18	0.5088	0.0057	0.1433	0.0042	2692	23	2674	13	2651	24	2706	75	109	892
S198/107-26	0.1861	0.0021	13.34	0.14	0.5200	0.0049	0.1455	0.0028	2708	19	2704	10	2699	21	2745	49	87	613
S198/107-27	0.1813	0.0025	12.39	0.13	0.4958	0.0042	0.1365	0.0013	2665	23	2635	10	2596	18	2586	22	71	541
S198/107-28	0.1833	0.0021	13.27	0.15	0.5250	0.0051	0.1516	0.0034	2683	20	2699	10	2720	22	2853	59	95	717
S198/107-30	0.1407	0.0018	7.76	0.09	0.4003	0.0040	0.1156	0.0030	2235	22	2204	11	2170	19	2211	55	60	455
S198/107-31	0.1846	0.0021	13.07	0.14	0.5135	0.0048	0.1420	0.0030	2694	19	2684	10	2671	20	2684	53	91	765
Sample: S204/2B																		
S204/2B-1	0.1996	0.0028	14.97	0.22	0.5441	0.0065	0.1344	0.0042	2823	24	2813	14	2801	27	2549	74	247	178
S204/2B-3	0.1684	0.0023	10.22	0.15	0.4401	0.0052	0.1265	0.0038	2542	24	2455	13	2351	23	2408	68	199	266
S204/2B-4	0.1307	0.0054	7.07	0.28	0.3921	0.0050	0.1114	0.0013	2107	75	2120	35	2132	23	2135	24	472	366
S204/2B-6	0.1303	0.0034	6.98	0.17	0.3886	0.0039	0.1105	0.0011	2102	47	2109	22	2116	18	2118	21	95	149
S204/2B-7	0.1168	0.0013	5.53	0.06	0.3434	0.0033	0.1009	0.0019	1908	21	1905	9	1903	16	1942	34	177	224
S204/2B-9	0.1984	0.0025	14.67	0.16	0.5361	0.0046	0.1503	0.0039	2813	21	2794	10	2767	19	2830	69	451	218

S204/2B-11	0.1751	0.0025	11.96	0.17	0.4956	0.0058	0.1229	0.0040	2607	24	2602	14	2595	25	2344	71	242	268
S204/2B-12	0.1409	0.0037	7.67	0.18	0.3948	0.0043	0.1114	0.0012	2238	46	2193	21	2145	20	2134	22	335	345
S204/2B-16	0.1510	0.0057	8.14	0.29	0.3909	0.0045	0.1095	0.0012	2358	66	2247	33	2127	21	2101	22	246	242
S204/2B-17	0.1442	0.0019	7.88	0.10	0.3966	0.0042	0.1178	0.0032	2278	23	2218	12	2153	20	2251	57	107	198
S204/2B-19	0.1552	0.0031	9.23	0.16	0.4311	0.0042	0.1205	0.0012	2404	35	2361	16	2311	19	2299	22	119	207
S204/2B-23	0.1604	0.0019	9.18	0.10	0.4151	0.0040	0.1140	0.0023	2460	20	2356	10	2238	18	2182	41	82	183
S204/2B-24	0.1832	0.0026	12.09	0.17	0.4785	0.0055	0.1346	0.0044	2682	24	2611	13	2521	24	2552	77	486	522
Sample: S204/23B																		
S204/23B-1	0.1146	0.0022	5.12	0.09	0.3238	0.0040	0.0804	0.0062	1874	35	1839	16	1808	19	1563	116	1.2	12
S204/23B-2	0.1156	0.0024	5.44	0.11	0.3412	0.0044	0.0884	0.0042	1889	39	1891	17	1892	21	1712	78	3.2	11
S204/23B-5	0.1139	0.0017	5.28	0.08	0.3361	0.0037	2.4256	0.1724	1863	28	1865	12	1868	18	24887	1017	0.1	16
S204/23B-7	0.1152	0.0027	5.30	0.12	0.3336	0.0042	0.2072	0.0300	1884	43	1869	19	1856	20	3806	503	0.2	7
S204/23B-8	0.1150	0.0024	5.36	0.11	0.3380	0.0046	0.1693	0.0414	1880	39	1879	18	1877	22	3161	716	0.2	13
S204/23B-9	0.1157	0.0017	5.40	0.07	0.3385	0.0034	0.0934	0.0048	1890	26	1884	11	1879	16	1805	89	0.9	10
S204/23B-11	0.1156	0.0022	5.38	0.10	0.3377	0.0039	0.1168	0.0275	1889	36	1882	15	1875	19	2233	498	0.1	6
S204/23B-13	0.1154	0.0034	5.30	0.15	0.3331	0.0056	0.5185	0.2378	1887	55	1869	24	1853	27	8442	3165	0.0	8
S204/23B-14	0.1156	0.0023	5.41	0.10	0.3393	0.0043	0.0834	0.0065	1890	37	1886	16	1883	21	1619	122	1.0	9
S204/23B-15	0.1169	0.0021	5.60	0.09	0.3475	0.0040	0.0841	0.0124	1909	33	1916	15	1923	19	1633	230	0.3	6
S204/23B-16	0.1149	0.0022	5.28	0.10	0.3330	0.0042	0.1284	0.0141	1879	35	1865	16	1853	20	2441	252	0.5	14
S204/23B-17	0.1165	0.0020	5.44	0.09	0.3385	0.0039	0.0506	0.0640	1903	32	1891	14	1880	19	1050	1363	0.1	9
S204/23B-18	0.1160	0.0025	5.39	0.11	0.3372	0.0045	0.1262	0.0228	1896	39	1884	17	1873	22	2403	409	0.2	9
S204/23B-23	0.1168	0.0027	5.55	0.12	0.3448	0.0048	0.2191	0.2182	1907	42	1908	19	1910	23	4004	3617	0.02	8
S204/23B-25	0.1149	0.0033	4.75	0.13	0.3000	0.0049	0.0436	0.0030	1878	54	1776	23	1691	24	862	59	3.8	8
Sample: S204/28																		
S204/28-1	0.2038	0.0025	15.16	0.19	0.5397	0.0059	0.1437	0.0035	2856	20	2825	12	2782	25	2713	61	359	1079
S204/28-2	0.2035	0.0024	15.45	0.18	0.5507	0.0058	0.0674	0.0016	2855	20	2844	11	2828	24	1319	30	283	392
S204/28-3	0.1914	0.0021	12.37	0.13	0.4687	0.0046	0.1229	0.0024	2755	19	2633	10	2478	20	2342	43	168	585
S204/28-4	0.2060	0.0023	15.98	0.16	0.5628	0.0052	0.1408	0.0028	2874	18	2876	10	2878	22	2663	49	211	747
S204/28-5	0.2077	0.0025	16.23	0.19	0.5669	0.0058	0.1682	0.0039	2887	20	2891	11	2895	24	3143	67	131	183
S204/28-6	0.2042	0.0025	15.51	0.20	0.5509	0.0060	0.1491	0.0039	2860	21	2847	12	2829	25	2809	69	682	1825
S204/28-7	0.2005	0.0024	15.05	0.18	0.5444	0.0057	0.1365	0.0032	2830	20	2818	11	2802	24	2585	57	161	619
S204/28-8	0.2032	0.0026	16.01	0.21	0.5715	0.0063	0.1671	0.0048	2852	22	2878	13	2914	26	3123	84	628	818
S204/28-9	0.1943	0.0025	14.61	0.18	0.5453	0.0052	0.1512	0.0043	2779	22	2790	11	2806	22	2847	76	119	108
S204/28-11	0.2040	0.0026	15.77	0.20	0.5607	0.0059	0.1143	0.0033	2859	21	2863	12	2870	24	2187	59	84	211
S204/28-13	0.1826	0.0029	12.53	0.21	0.4977	0.0064	0.1429	0.0056	2676	27	2645	16	2604	28	2700	98	128	215
S204/28-14	0.2056	0.0032	16.06	0.26	0.5668	0.0069	0.1581	0.0063	2871	26	2881	16	2895	29	2967	110	400	1028
S204/28-16	0.1938	0.0031	13.85	0.23	0.5186	0.0066	0.1555	0.0062	2775	27	2740	16	2693	28	2922	108	77	244
S204/28-18	0.1946	0.0023	14.03	0.15	0.5230	0.0046	0.1469	0.0034	2781	20	2752	10	2712	20	2771	60	101	451
S204/28-19	0.2059	0.0024	15.74	0.18	0.5547	0.0056	0.1524	0.0032	2873	19	2861	11	2845	23	2867	57	272	925
S204/28-20	0.1950	0.0032	14.74	0.24	0.5481	0.0065	0.1680	0.0070	2785	28	2798	16	2817	27	3139	120	56	205
S204/28-22	0.1874	0.0038	12.64	0.21	0.4891	0.0056	0.1342	0.0017	2720	34	2653	16	2567	24	2546	30	129	535

S204/28-23	0.2073	0.0040	16.04	0.32	0.5617	0.0075	0.1581	0.0083	2884	32	2879	19	2874	31	2967	144	102	150
S204/28-24	0.2043	0.0027	15.38	0.20	0.5462	0.0060	0.1540	0.0045	2861	22	2839	13	2809	25	2895	79	64	196
S204/28-25	0.2039	0.0030	15.77	0.23	0.5610	0.0062	0.1598	0.0055	2857	24	2863	14	2871	26	2996	97	602	1606
S204/28-27Core	0.2101	0.0028	16.75	0.22	0.5783	0.0063	0.1251	0.0036	2906	22	2920	13	2942	26	2383	64	314	864
S204/28-27Rim	0.1996	0.0027	11.90	0.15	0.4326	0.0044	0.0769	0.0023	2823	22	2597	12	2318	20	1498	43	84	315
S204/28-28	0.2111	0.0027	16.67	0.21	0.5726	0.0061	0.1576	0.0043	2914	21	2916	12	2918	25	2958	75	104	345
S204/28-29	0.2036	0.0029	15.79	0.23	0.5626	0.0066	0.1581	0.0053	2856	24	2864	14	2877	27	2967	93	145	730
S204/28-31	0.2119	0.0034	14.81	0.23	0.5073	0.0058	0.1369	0.0052	2920	26	2803	15	2645	25	2593	93	150	181
S204/28-32Core	0.2064	0.0028	16.34	0.22	0.5744	0.0063	0.1249	0.0038	2877	23	2897	13	2926	26	2379	69	167	381
S204/28-33	0.2042	0.0047	15.60	0.35	0.5542	0.0078	0.1483	0.0094	2860	38	2853	21	2842	32	2794	165	59	102
S204/28-34	0.2028	0.0032	15.76	0.26	0.5638	0.0069	0.1605	0.0065	2849	27	2862	16	2882	29	3008	114	139	542

Table DR2B. Th-U-Pb isotopic data from SHRIMP–II (after Kaulina et al., 2007)

Analysis #	$^{206}Pb_c$ %	U ppm	Th ppm	$^{232}Th/^{238}U$	$^{206}Pb^*$ ppm	$^{206}Pb/^{238}U$ age ± 1 σ	$^{207}Pb/^{206}Pb$ (1) age ± 1 σ	Discordancy, %	$^{207}Pb^*/^{235}U$ (1)	±%	$^{206}Pb^*/^{238}U$ (1)	±%	err corr
Sample: S204/2B													
Supposedly magmatic zircon (crystal with relics jf magmatic zoning)													
S204_2B.10.1	0,14	243	465	1,98	118	2891 ±50	2889 ± 11	0	16.22	2.2	0.566	2.1	,951
Zircons recrystallized under eclogite facies conditions (light sections, Th/U > 1.75													
S204_2B.3.1	0,15	496	857	1,79	211	2587 ±45	2787 ± 8	8	13.28	2.2	0.494	2.1	,971
S204_2B.4.1	0,35	520	1488	2,95	234	2706 ±46	2801 ± 11	3	14.16	2.2	0.522	2.1	,952
S204_2B.6.1	0,41	289	666	2,38	128	2665 ±47	2840 ± 14	7	14.24	2.3	0.512	2.1	,932
S204_2B.7.1	0,22	432	971	2,33	186	2617 ±45	2799 ± 9	7	13.58	2.2	0.501	2.1	,967
S204_2B.9.2	0,24	545	963	1,83	232	2588 ±45	2775 ± 9	7	13.2	2.2	0.494	2.1	,965
S204_2B.10.2	0,23	383	920	2,48	163	2584 ±45	2802 ± 9	8	13.39	2.2	0.493	2.1	,964
S204_2B.13.1	0,07	656	1458	2,30	267	2497 ±48	2750 ± 7	10	12.45	2.4	0.473	2.3	,982
Zircons recrystallized strongly under eclogite facies conditions (light sections, Th/U < 1.75													
S204_2B.1.1	1,61	86	76	0,92	30.7	2210 ±44	2290 ± 48	4	8.19	3.7	0.4089	2.4	,644
S204_2B.1.2	0,68	191	226	1,22	68.6	2234 ±41	2490 ± 27	11	9.32	2.7	0.4141	2.2	,810
S204_2B.2.1	0,47	162	162	1,03	62.1	2361 ±44	2531 ± 18	7	10.21	2.4	0.4423	2.2	,901
S204_2B.7.2	0,08	372	591	1,64	136	2280 ±43	2565 ±10	12	9.99	2.3	0.4243	2.2	,963
S204_2B.8.2	0,90	105	76	0,75	45.9	2622 ±50	2745 ± 43	5	13.17	3.5	0.502	2.3	,663
S204_2B.8.3	0,30	560	563	1,04	213	2359 ±42	2553 ± 13	8	10.33	2.3	0.4419	2.1	,934
S204_2B.9.1	0,76	189	142	0,78	72.3	2356 ±44	2561 ± 28	9	10.37	2.8	0.4413	2.2	,794
S204_2B.11.1	0,37	299	321	1,11	120	2461 ±43	2586 ± 13	5	11.08	2.3	0.4649	2.1	,939
S204_2B.15.1	0,07	309	368	1,23	130	2562 ±47	2675 ±11	4	12.28	2.3	0.488	2.2	,956
Thin light-gray rims of zircon crystals, Th/U < 0.5													
S204_2B.2.2	2,67	34	7	0,22	11.1	2013 ±69	2081 ±160	3	6.51	9.9	0.366	4	,405
S204_2B.4.2	3,69	54	5	0,09	22.4	2437 ±62	2527 ±130	4	10.57	8.3	0.459	3	,366
S204_2B.5.1	1,18	79	23	0,30	30.2	2336 ±57	2504 ± 70	7	9.92	5.1	0.437	2.9	,577
S204_2B.6.2	1,41	40	2	0,05	12.2	1949 ±49	2115 ±130	9	6.39	7.7	0.353	2.9	,379
S204_2B.12.1	1,42	29	8	0,27	11.7	2413 ±58	2576 ± 64	7	10.76	4.8	0.454	2.9	,603
S204_2B.14.1	1,39	66	8	0,12	19.1	1839 ±43	2094 ±87	14	5.9	5.7	0.3302	2.7	,476

Pb_c and Pb^* are common and radiogenic Pb, correspondingly,

Errors at standard calibration are from 0.37% to 0.91 %,

(1) correction for usual Pb was introduced using measured ^{204}Pb

Table DR3. Zircon Lu-Hf isotopic data

Analysis #	Measured Lu-Hf isotope ratios				Blichert-Toft et al. (1997) ^{176}Lu decay constant (1.93x10^{-11})					Scherer et al. (2001; 1.865x10^{-11})				Bizzarro et al. (2003; 1.983x10^{-11})			
	^{176}Hf/^{177}Hf	1 se	^{176}Lu/^{177}Hf	^{176}Yb/^{177}Hf	**Hf$_i$**	ε_{Hf}	1se	T_{DM} (Ga)	T_{DM}^c(Ga)	**Hf$_i$**	ε_{Hf}	T_{DM} (Ga)	T_{DM}^c(Ga)	**Hf$_i$**	ε_{Hf}	T_{DM} (Ga)	T_{DM}^c(Ga)
Sample: S198/107																	
S198/107-1	0.281117	0.000011	0.00013	0.004	0.281110	3.2	0.4	2.81	2.92	0.281111	1.0	2.91	3.09	0.281110	4.90	2.73	2.79
S198/107-2	0.281080	0.000009	0.00028	0.008	0.281065	2.5	0.3	2.87	2.99	0.281065	0.3	2.97	3.16	0.281064	4.26	2.79	2.86
S198/107-4	0.281075	0.000007	0.00026	0.008													
S198/107-5	0.281071	0.000009	0.00022	0.007	0.281059	1.3	0.3	2.88	3.03	0.281060	-0.9	2.98	3.20	0.281059	3.01	2.80	2.90
S198/107-6	0.281071	0.000007	0.00017	0.005	0.281062	2.3	0.2	2.87	3.00	0.281062	0.1	2.97	3.17	0.281062	4.05	2.80	2.87
S198/107-7	0.281068	0.000007	0.00028	0.007	0.281053	2.1	0.2	2.88	3.02	0.281053	-0.1	2.98	3.19	0.281052	3.86	2.81	2.88
S198/107-10	0.281127	0.000006	0.00029	0.009	0.281111	4.7	0.2	2.81	2.87	0.281112	2.5	2.91	3.04	0.281111	6.44	2.73	2.74
S198/107-11	0.281053	0.000008	0.00022	0.007	0.281041	1.9	0.3	2.90	3.03	0.281042	-0.2	3.00	3.21	0.281041	3.73	2.82	2.90
S198/107-12	0.281070	0.000010	0.00023	0.008													
S198/107-14	0.281080	0.000005	0.00021	0.007	0.281069	2.7	0.2	2.86	2.98	0.281069	0.5	2.96	3.15	0.281068	4.45	2.79	2.85
S198/107-15	0.281077	0.000006	0.00029	0.009	0.281062	1.2	0.2	2.87	3.03	0.281062	-0.9	2.97	3.20	0.281061	2.97	2.80	2.90
S198/107-16	0.281114	0.000008	0.00021	0.006	0.281103	3.7	0.3	2.82	2.91	0.281103	1.5	2.92	3.08	0.281102	5.46	2.74	2.78
S198/107-18	0.281114	0.000008	0.00021	0.006	0.281103	2.4	0.3	2.82	2.95	0.281103	0.3	2.92	3.12	0.281103	4.16	2.74	2.82
S198/107-20	0.281064	0.000009	0.00032	0.011	0.281047	2.7	0.3	2.89	3.01	0.281047	0.5	2.99	3.18	0.281046	4.46	2.81	2.87
S198/107-21	0.281052	0.000013	0.00016	0.004	0.281044	1.6	0.5	2.90	3.04	0.281044	-0.6	3.00	3.21	0.281043	3.36	2.82	2.91
S198/107-22	0.281151	0.000020	0.00018	0.006	0.281141	4.9	0.7	2.77	2.83	0.281142	2.7	2.87	3.00	0.281141	6.68	2.70	2.70
S198/107-23	0.281083	0.000017	0.00040	0.012	0.281063	-2.8	0.6	2.87	3.15	0.281064	-4.8	2.97	3.32	0.281063	-1.20	2.80	3.02
S198/107-24	0.281065	0.000009	0.00011	0.003	0.281059	1.1	0.3	2.88	3.04	0.281059	-1.1	2.98	3.21	0.281059	2.81	2.80	2.91
S198/107-25	0.281173	0.000015	0.00053	0.014	0.281145	4.8	0.5	2.77	2.83	0.281146	2.7	2.86	2.99	0.281144	6.58	2.69	2.70
S198/107-26	0.281058	0.000010	0.00021	0.006	0.281047	2.0	0.3	2.89	3.03	0.281047	-0.2	2.99	3.20	0.281047	3.78	2.81	2.89
S198/107-27	0.281055	0.000011	0.00021	0.006	0.281044	0.9	0.4	2.90	3.06	0.281044	-1.3	3.00	3.24	0.281043	2.60	2.82	2.93
S198/107-28	0.281086	0.000013	0.00013	0.004	0.281079	2.6	0.5	2.85	2.97	0.281080	0.4	2.95	3.14	0.281079	4.32	2.77	2.84
S198/107-30	0.281133	0.000014	0.00015	0.005	0.281126	-6.5	0.5	2.79	3.18	0.281127	-8.3	2.89	3.35	0.281126	-5.03	2.72	3.06
Sample: S204/2B																	
204/2B-1	0.281113	0.000012	0.00090	0.045	0.281063	5.3	0.4	2.87	2.91	0.281064	3.1	2.97	3.08	0.281061	7.15	2.79	2.78
204/2B-3	0.281143	0.000012	0.00059	0.027	0.281113	0.4	0.4	2.81	3.00	0.281114	-1.6	2.91	3.16	0.281113	2.03	2.73	2.87
204/2B-4	0.281143	0.000012	0.00059	0.027	0.281119	-9.8	0.4	2.81	3.29	0.281119	-11.4	2.91	3.45	0.281118	-8.44	2.73	3.16
204/2B-6	0.281281	0.000012	0.00184	0.086	0.281205	-6.8	0.4	2.72	3.10	0.281207	-8.4	2.81	3.25	0.281203	-5.56	2.65	2.99
204/2B-7	0.281100	0.000011	0.00076	0.039	0.281072	-16.2	0.4	2.88	3.52	0.281073	-17.6	2.98	3.68	0.281071	-14.95	2.80	3.39
204/2B-9	0.281226	0.000017	0.00151	0.081	0.281142	7.9	0.6	2.77	2.74	0.281145	5.7	2.86	2.90	0.281139	9.68	2.69	2.62
204/2B-11	0.281232	0.000016	0.00083	0.042	0.281189	4.6	0.6	2.71	2.78	0.281191	2.6	2.81	2.94	0.281188	6.31	2.64	2.66
204/2B-12	0.281288	0.000016	0.00121	0.045	0.281235	-2.6	0.6	2.66	2.94	0.281237	-4.3	2.76	3.10	0.281233	-1.14	2.59	2.83
204/2B-16	0.281144	0.000010	0.00124	0.048	0.281086	-5.0	0.4	2.86	3.19	0.281088	-6.8	2.96	3.35	0.281085	-3.49	2.78	3.06
204/2B-17	0.281144	0.000010	0.00124	0.048	0.281088	-6.8	0.4	2.86	3.24	0.281090	-8.6	2.96	3.40	0.281087	-5.37	2.78	3.11

204/2B-19	0.281235	0.000011	0.00171	0.064	0.281154	-1.5	0.4	2.77	3.01	0.281157	-3.3	2.87	3.16	0.281152	0.03	2.70	2.89
204/2B-23	0.281152	0.000013	0.00112	0.052	0.281093	3.0	0.5	2.84	2.94	0.281095	0.9	2.94	3.11	0.281091	4.72	2.76	2.82
204/2B-24	0.281289	0.000015	0.00108	0.041													
***Sample: S204/2B - calculated using 2820Ma crystallisation age**																	
204/2B-1	0.281113	0.000012	0.00090	0.045	0.281063	5.3	0.4	2.87	2.91	0.281065	3.0	2.97	3.08	0.281061	7.1	2.79	2.78
204/2B-3	0.281143	0.000012	0.00059	0.027	0.281110	6.9	0.4	2.81	2.80	0.281111	4.7	2.91	2.97	0.281109	8.8	2.73	2.68
204/2B-4	0.281143	0.000012	0.00059	0.027	0.281110	6.9	0.4	2.81	2.80	0.281111	4.7	2.91	2.97	0.281109	8.8	2.73	2.68
204/2B-6	0.281281	0.000012	0.00184	0.086	0.281178	9.4	0.4	2.72	2.65	0.281181	7.2	2.81	2.81	0.281175	11.1	2.65	2.53
204/2B-7	0.281100	0.000011	0.00076	0.039	0.281058	5.1	0.4	2.88	2.92	0.281059	2.8	2.98	3.09	0.281057	6.9	2.80	2.79
204/2B-9	0.281226	0.000017	0.00151	0.081	0.281142	8.1	0.6	2.77	2.73	0.281144	5.9	2.86	2.90	0.281139	9.8	2.69	2.61
204/2B-11	0.281232	0.000016	0.00083	0.042	0.281186	9.6	0.6	2.71	2.64	0.281187	7.4	2.81	2.80	0.281184	11.5	2.64	2.51
204/2B-12	0.281288	0.000016	0.00121	0.045	0.281221	10.9	0.6	2.66	2.56	0.281223	8.7	2.76	2.72	0.281219	12.7	2.59	2.44
204/2B-16	0.281144	0.000010	0.00124	0.048	0.281075	5.7	0.4	2.86	2.88	0.281077	3.5	2.96	3.05	0.281073	7.5	2.78	2.75
204/2B-17	0.281144	0.000010	0.00124	0.048	0.281075	5.7	0.4	2.86	2.88	0.281077	3.5	2.96	3.05	0.281073	7.5	2.78	2.75
204/2B-19	0.281235	0.000011	0.00171	0.064	0.281140	8.0	0.4	2.77	2.74	0.281143	5.8	2.87	2.90	0.281137	9.8	2.70	2.62
204/2B-23	0.281152	0.000013	0.00112	0.052	0.281090	6.2	0.5	2.84	2.85	0.281092	4.0	2.94	3.02	0.281088	8.0	2.76	2.72
204/2B-24	0.281289	0.000015	0.00108	0.041	0.281229	11.2	0.5	2.65	2.54	0.281231	9.0	2.75	2.70	0.281227	13.0	2.58	2.42
Sample: S204/23B																	
S-204/23B-1	0.281492	0.000014	0.00088	0.042	0.281460	-3.2	0.5	2.37	2.70	0.281461	-4.6	2.45	2.84	0.281459	-2.00	2.31	2.60
S-204/23B-2	0.281317	0.000013	0.00118	0.054	0.281273	-9.4	0.5	2.62	3.10	0.281275	-10.9	2.71	3.24	0.281272	-8.27	2.55	2.98
S-204/23B-5	0.281681	0.000015	0.00061	0.019	0.281659	3.6	0.5	2.11	2.27	0.281660	2.2	2.18	2.40	0.281658	4.82	2.05	2.18
S-204/23B-7	0.281911	0.000013	0.00001	0.000	0.281911	13.1	0.5	1.78	1.70	0.281911	11.6	1.84	1.81	0.281911	14.30	1.73	1.62
S-204/23B-8	0.281938	0.000011	0.00001	0.000	0.281938	13.9	0.4	1.74	1.65	0.281938	12.4	1.80	1.75	0.281938	15.16	1.69	1.57
S-204/23B-9	0.281329	0.000020	0.00101	0.048	0.281291	-8.8	0.7	2.60	3.06	0.281293	-10.2	2.69	3.20	0.281290	-7.60	2.53	2.94
S-204/23B-11	0.281900	0.000010	0.00003	0.001	0.281899	12.8	0.4	1.79	1.73	0.281899	11.3	1.85	1.83	0.281899	14.00	1.74	1.64
S-204/23B-13	0.281176	0.000014	0.00104	0.051	0.281137	-14.3	0.5	2.80	3.39	0.281139	-15.8	2.90	3.55	0.281136	-13.14	2.72	3.27
S-204/23B-15	0.281294	0.000016	0.00117	0.054	0.281250	-9.8	0.6	2.65	3.13	0.281252	-11.3	2.75	3.28	0.281249	-8.60	2.58	3.02
S-204/23B-16	0.281665	0.000017	0.00041	0.017	0.281650	3.7	0.6	2.12	2.28	0.281650	2.2	2.19	2.41	0.281649	4.89	2.06	2.19
S-204/23B-17	0.281441	0.000019	0.00160	0.080	0.281381	-5.3	0.7	2.49	2.85	0.281383	-6.7	2.57	2.99	0.281380	-4.11	2.42	2.75
S-204/23B-18	0.281877	0.000008	0.00000	0.000	0.281877	12.2	0.3	1.82	1.77	0.281877	10.6	1.88	1.88	0.281877	13.39	1.77	1.69
S-204/23B-23	0.281850	0.000010	0.00000	0.000	0.281850	11.5	0.4	1.86	1.82	0.281850	9.9	1.92	1.93	0.281850	12.70	1.81	1.74
S-204/23B-25	0.281251	0.000015	0.00122	0.052	0.281206	-12.1	0.5	2.71	3.25	0.281208	-13.5	2.81	3.40	0.281205	-10.92	2.64	3.13
Sample: S204/28																	
S204/28-1	0.281033	0.000010	0.00041	0.018	0.281010	4.2	0.4	2.94	3.00	0.281010	1.9	3.04	3.18	0.281009	6.10	2.86	2.87
S204/28-2	0.281023	0.000010	0.00054	0.019	0.280993	3.6	0.4	2.96	3.04	0.280994	1.3	3.06	3.21	0.280992	5.47	2.88	2.90
S204/28-3	0.281031	0.000015	0.00036	0.012	0.281011	1.9	0.5	2.94	3.07	0.281012	-0.3	3.04	3.24	0.281011	3.67	2.86	2.94
S204/28-4	0.281040	0.000009	0.00055	0.024	0.281009	4.6	0.3	2.94	2.99	0.281010	2.3	3.04	3.16	0.281008	6.51	2.86	2.85
S204/28-5	0.281049	0.000015	0.00039	0.016	0.281027	5.6	0.5	2.92	2.94	0.281027	3.3	3.02	3.11	0.281026	7.48	2.84	2.81
S204/28-6	0.281029	0.000017	0.00072	0.033	0.280988	3.6	0.6	2.97	3.04	0.280990	1.3	3.07	3.22	0.280987	5.43	2.89	2.91
S204/28-7	0.281035	0.000011	0.00074	0.035	0.280994	3.0	0.4	2.96	3.05	0.280995	0.8	3.06	3.23	0.280992	4.87	2.88	2.92

S204/28-8	0.281036	0.000016	0.00051	0.020	0.281007	4.1	0.6	2.94	3.01	0.281008	1.8	3.04	3.18	0.281006	5.92	2.86	2.87
S204/28-11	0.281014	0.000013	0.00042	0.017	0.280990	3.6	0.5	2.96	3.04	0.280991	1.3	3.07	3.22	0.280990	5.49	2.88	2.91
S204/28-13	0.281055	0.000025	0.00025	0.007	0.281042	1.0	0.9	2.90	3.06	0.281042	-1.1	3.00	3.23	0.281041	2.80	2.82	2.93
S204/28-14	0.281025	0.000013	0.00051	0.021	0.280996	4.1	0.5	2.96	3.02	0.280997	1.8	3.06	3.19	0.280995	6.00	2.88	2.88
S204/28-18	0.281045	0.000014	0.00038	0.017	0.281024	2.9	0.5	2.92	3.02	0.281025	0.7	3.02	3.20	0.281023	4.76	2.84	2.89
S204/28-19	0.281013	0.000014	0.00074	0.028	0.280971	3.3	0.5	2.99	3.07	0.280972	1.0	3.09	3.25	0.280970	5.13	2.91	2.94
S204/28-20	0.281141	0.000013	0.00067	0.024	0.281104	5.9	0.5	2.82	2.84	0.281105	3.7	2.92	3.01	0.281103	7.69	2.74	2.72
S204/28-23	0.281051	0.000014	0.00041	0.012	0.281028	5.6	0.5	2.92	2.94	0.281029	3.2	3.02	3.11	0.281027	7.45	2.84	2.81
S204/28-25	0.281061	0.000011	0.00052	0.022	0.281031	5.0	0.4	2.91	2.95	0.281032	2.8	3.01	3.12	0.281031	6.90	2.83	2.82
S204/28-31	0.281044	0.000025	0.00027	0.009	0.281028	6.4	0.9	2.91	2.91	0.281029	4.1	3.02	3.09	0.281028	8.37	2.84	2.78
S204/28-34	0.281059	0.000024	0.00075	0.025	0.281017	4.3	0.8	2.93	2.99	0.281018	2.1	3.03	3.16	0.281015	6.16	2.85	2.86

Table DR4. Calculated P-T conditions for the inferred equilibria in the studied samples (also see Figure 4)

Lithology, sample	*Stage*, assemblage	Calibration	*T* (°C)	*P* (GPa)
Shirokaya Salma locality				
Eclogite	*Retrograde*			
S-198/107	Grt-Cpx-Pl-Qtz	GCPQ (TPF)	723	1.15
	Cpx-Pl-Qtz	McCarthy, Patiño Douce, equation 5, (1998)	(750)	1.06
	Cpx-Pl-Qtz	McCarthy, Patiño Douce, equation 7, (1998)	(750)	0.97
Uzkaya Salma locality				
Eclogite	*Peak*			
SB-812	Cpx-Pl-Qtz	Holland (1980)	(700)	1.28
	Grt-Cpx	Powell (1985)	698	(1.30)
	Retrograde			
	Cpx-Pl-Qtz	McCarthy, Patiño Douce, equation 5, (1998)	(750)	1.03
	Cpx-Pl-Qtz	McCarthy, Patiño Douce, equation 7, (1998)	(750)	0.95
Eclogite,	*Prograde (?)*			
M2a	Included in garnet			
	Grt-Hbl	Powell (1985)	687	
	Grt-Hbl	Lavrentieva and Perchuk (1989)	704	
	Grt-Cpx	Powell (1985)	707	(1.0)
	Peak			
	Cpx-Pl-Qtz	Holland (1980)	(750)	(1.4)
	Retrograde			
	Grt-Cpx-Pl-Qtz	GCPQ (TPF)	747	1.19
	Cpx-Pl-Qtz	McCarthy, Patiño Douce, equation 5, (1998)	(750)	1.32
	Cpx-Pl-Qtz	McCarthy, Patiño Douce, equation 7, (1998)	(750)	1.2
Eclogite,	*Prograde (?)*			
S204/16	Included in garnet			
	Grt-Hbl	Powell (1985)	643	
	Grt-Hbl	Lavrentieva and Perchuk (1989)	670	
	Hbl-Pl-Qtz	Holland and Blundy (1994)	650	(0.7)
	Hbl-Pl	Holland and Blundy (1994)	490	(0.7)
	Cpx-Pl-Qtz	McCarthy, Patiño Douce, equation 5, (1998)	(700)	0.74
	Cpx-Pl-Qtz	McCarthy, Patiño Douce, equation 7, (1998)	(700)	0.66
Fe-Ti	*Retrograde*			
eclogite,	Grt-Cpx-Pl-Qtz	GCPQ (TPF)	689	1.0
S204/3	Cpx-Pl-Qtz	McCarthy, Patiño Douce, equation 5, (1998)	(700)	(0.85)
	Cpx-Pl-Qtz	McCarthy, Patiño Douce, equation 7, (1998)	(700)	(0.75)

Ky-Grt-Bt	*Peak*			
plagiogranite	Grt-Bt	GB (TPF)	732	(1.4)
S204/28	Grt-Ky-Pl-Qtz	Koziol and Newton (1989)	(700)	1.35
	Retrograde			
	Grt-Bt	GB (TPF)	643	(1.0)
	Grt-Ky-Pl-Qtz	Koziol and Newton (1989)	600	0.91

Abbreviations for the self-consistent calibrations of the program TPF (Fonarev et al., 1991; Konilov, 1999; Maaskant, 2004): GCPQ is Grt-Cpx-Pl-Qtz geothermobarometer combined of Grt-Cpx-Pl-Qtz geobarometer (Fonarev et al., 1994) and Grt-Cpx geothermometer (Powell, 1985); GB is Grt-Bt geothermometer, averaged of (Perchuk and Lavrent'eva, 1983) and (Holdaway and Lee, 1977).

References to Table DR4:

Fonarev, V.I., Graphchikov, A.A., and Konilov, A.N., 1991. A consistent system of geothermometers for metamorphic complexes. International Geology Review 33, 8, 743-783.

Fonarev, V.I., Graphchikov, A.A., and Konilov A.N., 1994. Experimental studies of equilibriums with minerals of variable composition and geological thermobarometry. Experimental problems of geology. Moscow, Nauka. 323-355 (in Russian).

Holdaway, M.J., and Lee, S.M., 1977. Fe-Mg cordierite stability in high-grade pelitic rocks based on experimental, theoretical, and natural observations. Contrib. Mineral. Petrol. 63, 175-198.

Holland, T.J.B., 1980.The reaction albite=jadeite+quartz determined experimentally in the range 600–1200ºC. Am. Min. 65, 129–134.

Holland, T., and Blundy J., 1994. Non-ideal interactions in calcic amphiboles and their bearing on amphibole-plagioclase thermometry. Contrib. Miner. Petrol. 116, 433-447.

Konilov, A.N., 1999. Testing of the consistent system of geothermometers and geobarometers of the program TPF. Experiment in GeoSciences 8, 1, 60-62.

Koziol, A.M., and Newton, R.C., 1989. Grossular activity-composition relationships in ternary garnets determined by reversed displaced-equilibrium experiments. Contrib. Miner. Petrol. 103, 423-433.

Lavrent'eva, I.V. and Perchuk, L.L., 1989. An experimental study of the amphibole-garnet equilibrium: calcium free system Dokl. Akad. Nauk USSR 306, 173-175 (in Russian).

Maaskant, P., 2004. Thermobarometry of the Furua granulites, Tanzania: a comparative study. Neue Jb. Miner. Abh., Stuttgart, 180, 65-100.

McCarthy, T.C., and Patiño Douce, A.E., 1998. Empirical calibration of the silica-Ca-tschermak's-anorthite (SCAn geobarometer). J. Metamorph. Geology 6, 671-682.

Perchuk, L.L., and Lavrent'eva, I.V., 1983. Experimental investigation of exchange equilibria in the system cordierite-garnet-biotite. Advances in Physical Geochemistry 3, 199-239.

Powell, R., 1985. Regression diagnostic and robust regression in geothermometer/geobarometer calibration: the garnet-clinopyroxene geothermometer revised. J. Metamorph. Geology 3, 231-243.

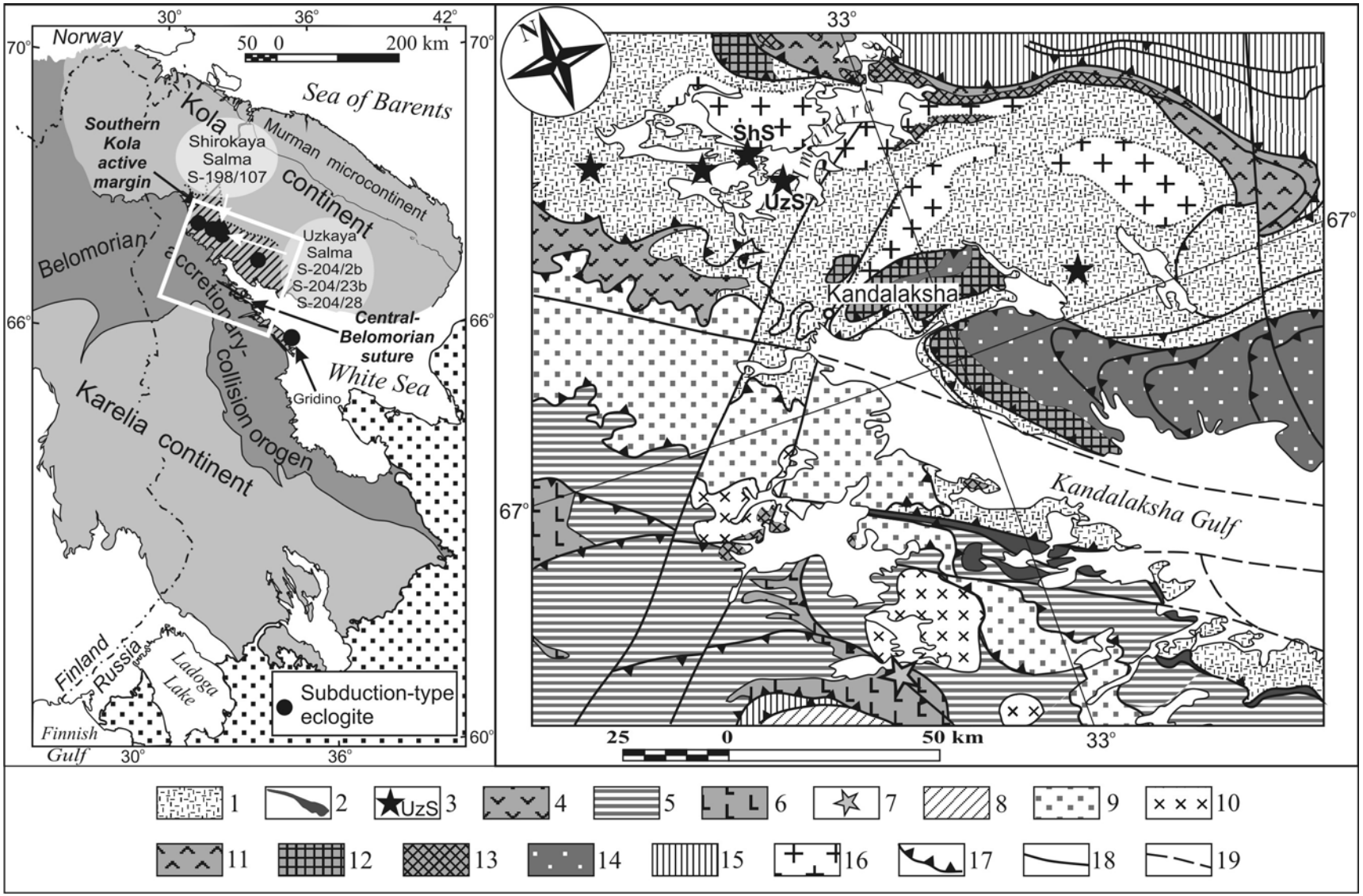

Figure DR1. Regional tectonic map of the eastern Fennoscandian Shield (left) and geologic sketch-map of the area of the Archean eclogite localities (right), where

Meso-Neoarchean:

(1) – Keret' tectonic nappe at southern margin of the Archean Kola continent, 2.89-2.70 Ga TTG;

(2) – ≥2.88-2.85 Ga Central Belomorian suture zone;

(3) – eclogite localities (UzS – Uzkaya Salma and ShS – Shirokaya Salma);

(4) – 2.78-2.74 Ga island arc type greenstones;

(5-7) – Belomorian orogen: 3.1-2.77 Ga TTG (5), 2.80-2.77 Ga greenstones (6), and 2.78 Ga Iringora ophiolites (see Shchipansky et al., 2004) (7);

(8) – Karelia continent, 3.5-2.7 Ga TTG.

Neoarchean:

(9) – 2.74-2.68 Ga Chupa granulite-gneiss belt;

(10)– 2.73-2.71 Ga enderbite bodies;

(11) – 2.72-2.66 Ga greenstones.

Paleoproterozoic:

(12-13) – 2.53-2.42 Ga intrusive bodies: layred mafic-ultramafics (12) and gabbro-anorthosites (13);

(14) – ca. 1.95 Ga Lapland-Kolvitsa granulite-gneiss belt;

(15) – Paleoproterozoic volcano-sedimentary belts;

(16) – late Paleoproterozoic granite-gneiss domes;

(17-19) – faults: overthrusts (17), normal faults and strike-slip faults (18), faults beneath water areas (19).

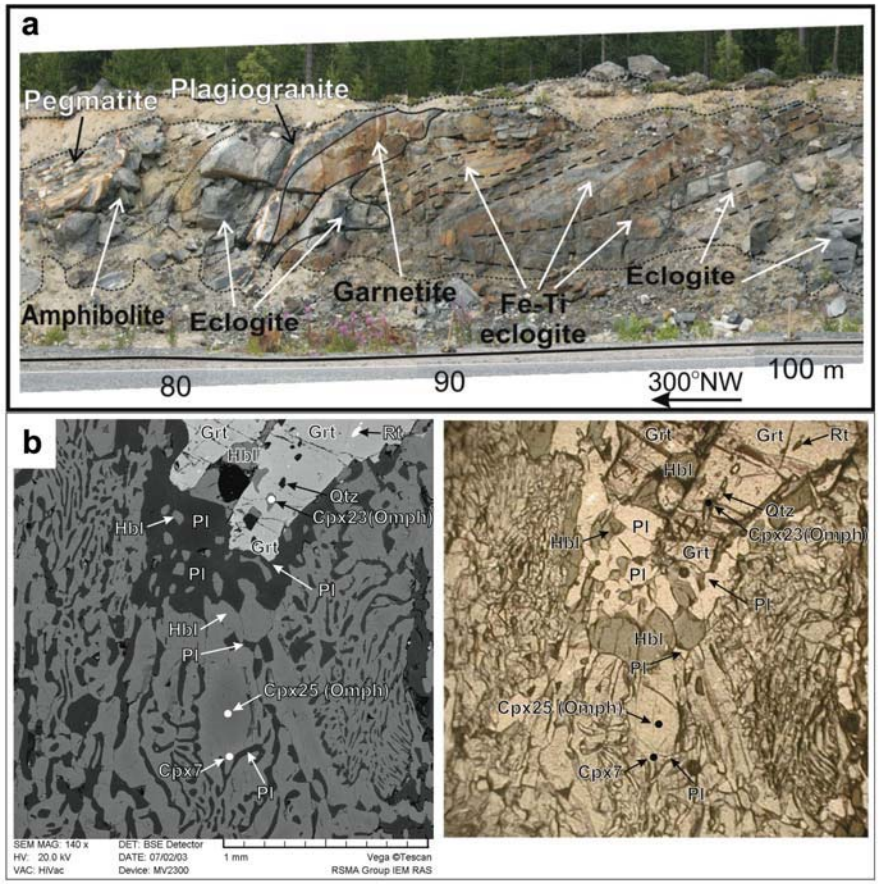

Figure DR2. Geological and petrological features of the Salma eclogites. a) A photo of the UzS body in outcrop; b) almandine-pyrope garnets set in a matrix of vermicular clinopyroxene-plagioclase symplectite and locally preserved omphacite; backscattered electron image (left) and transmitted light image (right).
Inclusions of the relic low-T minerals in the Salma eclogite as an evidence of the prograde metamorphic evolution: c) atoll type garnet within Cpx-Pl symplectite microphoto (left) with the inset showing enlarged BSE image of the central part of atoll, and a compositional profile (right), where shaded area corresponds to “lagoon” of atoll; d) BSE image of the atoll type garnet (left) with inclusions marked by white arrows for Ab (albite) and Pmp (pumpellyite), and a compositional profile (right), where shaded area corresponds to a zone with relics of Ab, Act (actinolite) and Pmp, scale bar is 2 mm long; e) SE image showing quartz needle-shaped inclusions (rods) in omphacite, width of a field of view is 200 μm; f) photomicrograph of the quartz needle-shaped inclusions in omphacite, scale bar is 50 μm long. Similar inclusions are

known in the UHP assemblages, e.g., in Kokchetav massif (Katayama, Maruyama, 2009), Pohorje, Eastern Alps (Janák et al., 2004), Alpe Arami (Dobrzhinetskaya et al., 2002), Blumenau eclogite, Erzgebirge (Chopin, Ferraris, 2003). This feature permits suggestion that peak conditions in the history of the Salma eclogite could reach much higher pressure then 1.4 GPa that were fixed in these rocks to-day. Also see Table DR4 and Fig. 4.

References in Data Repository Figure DR2:

Chopin, C., Ferraris, G. Mineral chemistry and mineral reactions in UHPM rocks. In: (Carswell D.A., Compagnoni R., Rolfo F., Eds.) Ultrahigh Pressure Metamorphism. EMU Notes in Mineralogy, Vol. 5 (2003), Chapter 7, 191–227.

Dobrzhinetskaya, L.F., Schweinehage, R., Massonne, H.-J., Green, H.W. Silica precipitates in omphacite from eclogite at Alpe Arami, Switzerland: evidence of deep subduction. J. metamorphic Geol., 2002, 20, 481–492.

Janák, M., Froitzheim, N., Lupták, B., Vrabec, M., Krogh Ravna, E.J. First evidence for ultrahigh-pressure metamorphism of eclogites in Pohorje, Slovenia: Tracing deep continental subduction in the Eastern Alps. Tectonics, 2004, v.23, TC5014, doi: 10.1029/2004TC001641.

Katayama, I., Maruyama, S. Inclusion study in zircon from ultrahigh-pressure metamorphic rocks in the Kokchetav massif: an excellent tracer of metamorphic history. Journal of the Geological Society, London, 2009, v.166, no.4, 783–796, doi: 10.1144/0016-76492008-019.

Shchipansky, A.A., Samsonov, A.V., Bibikova, E.V., Babarina, I.I., Konilov, A.N., Krylov, K.K., Slabunov, A.I., Bogina, M.M. 2.8 Ga boninite-hosting partial suprasubduction zone ophiolite sequences from the North Karelian greenstone belt, NE Baltic Shield, Russia. In: Precambrian ophiolites and related rocks (T. Kusky – Ed.). 2004. Development in Precambrian Geology, 13. Elsevier, Amsterdam, Chapter 14, 425-486.

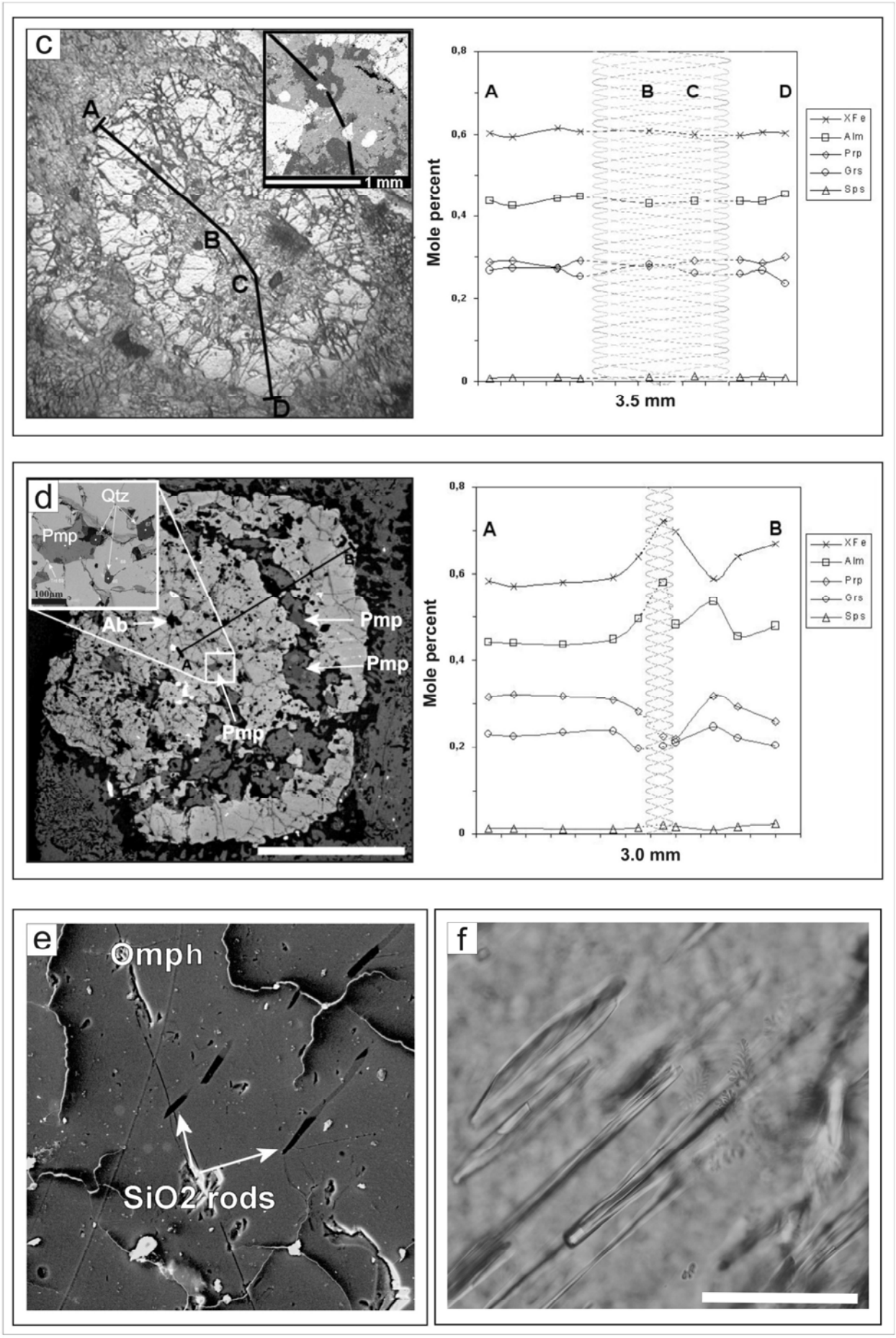

Figure DR2 (c,d,e,f)

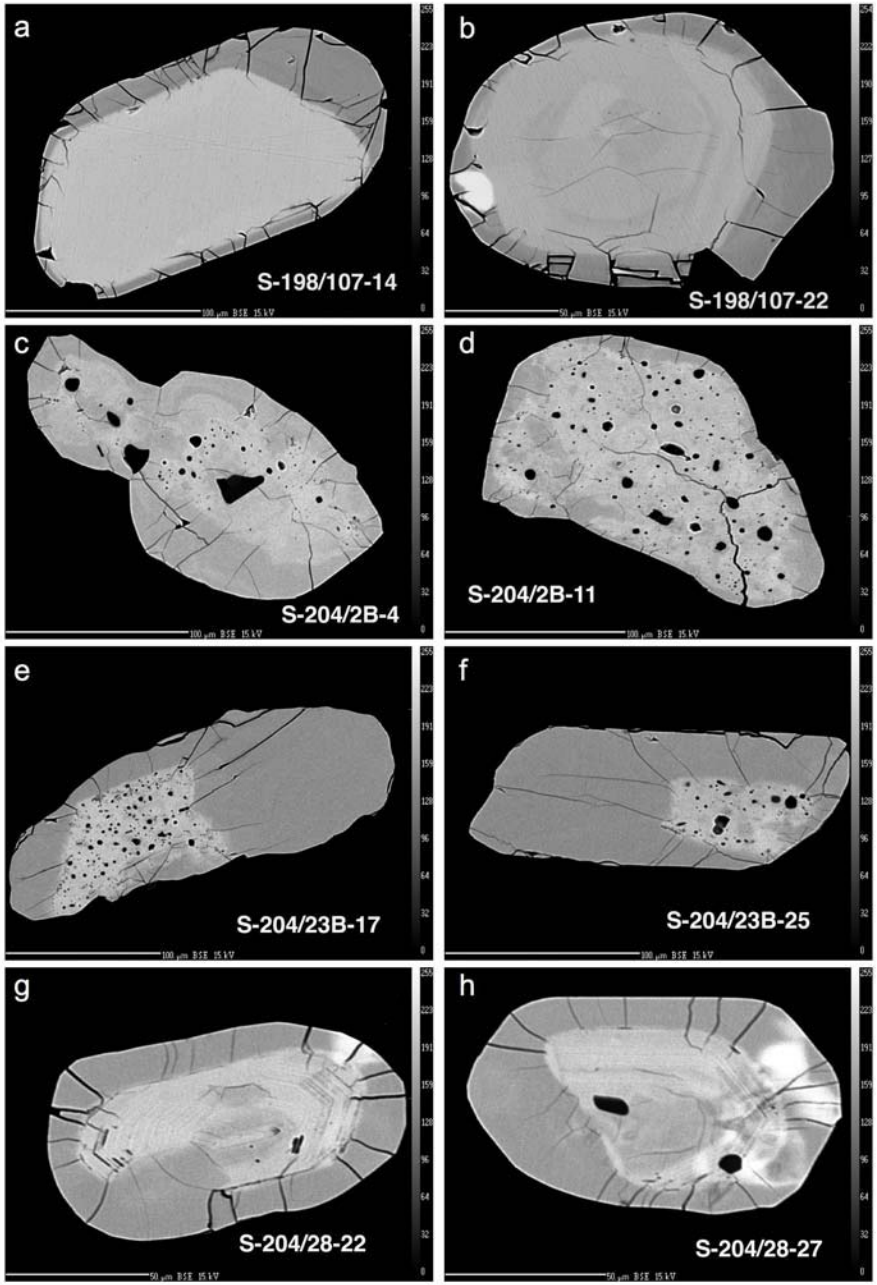
a
S-198/107-14
b
S-198/107-22
c
S-204/2B-4
d
S-204/2B-11
e
S-204/23B-17
f
S-204/23B-25
g
S-204/28-22
h
S-204/28-27

Figure DR3

Figure DR3. Backscattered electron/cathodoluminescence images of representative zircon grains from the analysed samples. Scale bar: 100 μm for images a, c, d, e and f and 50 μm for images b, g and h. See text for explanations.